# Assessing the Impact of Electrode Structure on the Thermal Behaviour of 18650 Li-ion Batteries: A Physics-Based Modelling Approach

AHMAD ABDULLAH MUJAHID

SUPERVISOR

Dr. Williams Agyei Appiah

Dr. Abu Shadat Muhammad Sayem

Dr. Souman Rudra

**University of Agder, [2024]**

Faculty of Engineering and Science

Department of Engineering Sciences

## Abstract

Thermal management is one of the significant concerns of the commercial cylindrical 18650 Li-ion battery, as it can affect battery performance, lifespan, and safety. In the present work, we develop and implement an experimentally validated pseudo-2D lithium-ion battery model electrochemical coupled with the thermal model to investigate the electrochemical and thermal behaviour of the commercial 18650 lithium iron phosphate battery made of $LiFePO_4$ cathode and graphite anode. We integrate a bio-inspired electrolyte channel design into electrodes to improve thermal performance, especially during high C-rate discharging. This proposed model is established and simulated by using COMSOL Multiphysics 6.2. Four cell geometries were analysed for this work: one conventional cell, channel in the positive electrode, channel in the negative electrode, and channel in both electrodes. We investigate the effects of electrolyte channel width, thickness, and channel number for designed geometries on electrochemical and thermal performance. The findings indicate that a specific set of channel geometrical parameters can significantly reduce battery temperature during discharging. The addition of an electrolyte channel into the negative electrode with 50 nm width, 5 µm thickness, and 5 number channels provides optimum thermal performance. It decreases temperature for 2C and 3C by 8.4% and 5.45%, respectively. This study provides an electrode design strategy to improve the thermal performance of commercial 18650 Li-ion batteries.

## Abstrakt

Termisk styring er en av de viktigste utfordringene for kommersielle sylindriske 18650 Li-ion-batterier, da det kan påvirke batteriets ytelse, levetid og sikkerhet. I dette arbeidet utvikler og implementerer vi en eksperimentelt validert pseudo-2D litium-ion-batterimodell som kobler elektrokjemiske og termiske egenskaper for å undersøke oppførselen til det kommersielle 18650 litiumjernfosfatbatteriet ($LiFePO_4$) med grafittanode. Vi integrerer en bioinspirert elektrolyttkanaldesign i elektrodene for å forbedre den termiske ytelsen, spesielt under utlading ved høye C-rater. Den foreslåtte modellen er etablert og simulert ved bruk av COMSOL Multiphysics 6.2. Fire cellegeometrier ble analysert i dette arbeidet: en konvensjonell celle, en celle med kanal i den positive elektroden, en celle med kanal i den negative elektroden, og en celle med kanal i begge elektrodene. Vi undersøker effekten av elektrolyttkanalens bredde, tykkelse og antall kanaler på elektrokjemisk og termisk ytelse i de ulike geometriene. Resultatene viser at en spesifikk kombinasjon av geometriske parametere for kanalene kan redusere batteriets temperatur betydelig under utlading. Tilsetningen av en elektrolyttkanal i den negative elektroden, med en bredde på 50 nm, en tykkelse på 5 µm, og fem kanaler, gir optimal termisk ytelse. Dette reduserer temperaturen ved 2C og 3C med henholdsvis 8.4 % og 5.45 %. Denne studien presenterer en strategi for elektrodesign som kan forbedre den termiske ytelsen til kommersielle 18650 Li-ion-batterier.

## Preface

This thesis work was conducted under the project "Collaborative Action for Improving Educational Capacities in Renewable Energy to mitigate climate crisis (CARE)" between Chittagong University of Engineering & Technology (CUET), Bangladesh and University of Agder (UIA), Norway (Collaboration Agreement No. NORPART-2021/10355).

I would like to express my deepest gratitude to my supervisors, Dr. Williams Agyei Appiah, for his outstanding guidance, unwavering support, and invaluable advice throughout the course of this project. His profound knowledge, patience, and encouragement have been instrumental in shaping this work and in broadening my understanding of the subject matter. I am especially grateful for his time and effort in providing constructive feedback and continuously motivating me to aim for excellence. His mentorship has not only guided me academically but has also inspired me on a personal level to persevere and approach challenges with confidence. This project would not have been possible without their consistent support and willingness to share their expertise, and I am truly fortunate to have had the privilege of working under their supervision.

I would like to extend my heartfelt gratitude to Dr. Abu Shadat Muhammad Sayem and Dr. Souman Rudra for their invaluable advice, guidance, and unwavering support throughout my time working on the CARE project. Their insights and mentorship have been instrumental in enabling me to successfully complete my work under this initiative.

Lastly, my father, Mahmud Hossain, and my mother, Jannatul Ferdousi and other family members deserve thanks for their unconditional love, mental support, and kind words, which served me well.

I want to express my heartfelt appreciation to everyone for their assistance with technical matters and their moral encouragement and helpful advice in the thesis work.

Ahmad Abdullah Mujahid

University of Agder (uiA),

Grimstad, Norway

December 2024

## Individual/group Mandatory Declaration

The individual student or group of students is responsible for the use of legal tools, guidelines for using these and rules on source usage. The statement will make the students aware of their responsibilities and the consequences of cheating. Missing statement does not release students from their responsibility.

| | | |
|---|---|---|
| 1. | I/We hereby declare that my/our report is my/our own work and that I/We have not used any other sources or have received any other help than mentioned in the thesis. | ☒ |
| 2. | I/we further declare that this thesis:<br>- has not been used for another exam at another department/university/university college in Norway or abroad;<br>- does not refer to the work of others without it being stated;<br>- does not refer to own previous work without it being stated;<br>- have all the references given in the literature list;<br>- is not a copy, duplicate or copy of another's work or manuscript. | ☒ |
| 3. | I/we am/are aware that violation of the above is regarded as cheating and may result in cancellation of exams and exclusion from universities and colleges in Norway, see Universitets- og høgskoleloven §§4-7 og 4-8 og Forskrift om eksamen §§ 31. | ☒ |
| 4. | I/we am/are aware that all submitted theses may be checked for plagiarism. | ☒ |
| 5. | I/we am/are aware that the University of Agder will deal with all cases where there is suspicion of cheating according to the university's guidelines for dealing with cases of cheating. | ☒ |
| 6. | I/we have incorporated the rules and guidelines in the use of sources and references on the library's web pages. | ☒ |

## Publishing Agreement

Authorization for electronic publishing of the thesis.

Author(s) have copyrights of the thesis. This means, among other things, the exclusive right to make the work available to the general public (Åndsverkloven. §2).

All theses that fulfill the criteria will be registered and published in Brage Aura and on UiA's web pages with author's approval.

Theses that are not public or are confidential will not be published.

I hereby give the University of Agder a free right to

make the task available for electronic publishing: ☒JA ☐NEI

Is the thesis confidential? ☐JA ☒NEI

(confidential agreement must be completed and signed by the Head of the Department)

- If yes:

Can the thesis be published when the confidentiality period is over? ☒JA ☐NEI

Is the task except for public disclosure? ☐JA ☒NEI

(contains confidential information. see Offl. §13/Fvl. §13)

Table of Contents

Abstract ..... i
Abstrakt ..... ii
Preface ..... iii
Individual/group Mandatory Declaration ..... iv
Publishing Agreement ..... v
Table of Contents ..... vi
List of Figures ..... x
List of Tables ..... xii
Notation ..... xiii
Abbreviations ..... xvi
Chapter 1 ..... 1
Introduction ..... 1
1.1 Background ..... 1
1.2 Problem Statement ..... 5
1.4 Thesis Outline ..... 6
Chapter 2 ..... 7
Theory ..... 7
2.1 Electrochemical Cells ..... 7
2.1.1 Battery ..... 7
2.1.2 Types of Battery ..... 7
2.1.2.1 Primary Batteries: ..... 7
2.1.2.2 Secondary Batteries: ..... 7
2.2 Battery terminology ..... 8
2.2.1 Battery Capacity & power ..... 8
2.2.2 C-rate ..... 8
2.2.3 State of Health (SoH) ..... 8
2.2.4 State of Charge (SoC) ..... 9
2.2.5 Depth of Charge (DoD) ..... 9
2.2.6 Open Circuit Voltage (OCV) ..... 9

2.2.7 Terminal Voltage (V) ..... 10
2.2.8 Nominal Voltage (V) ..... 10
2.2.9 Cut-off Voltage (V) ..... 10
2.2.10 Energy or Nominal Energy (Wh) ..... 10
2.2.11 Specific Energy (Wh/kg) ..... 10
2.2.12 Specific Power (W/kg) ..... 10
2.2.13 Energy Density (Wh/L) ..... 11
2.2.14 Power Density (W/L) ..... 11
2.3 Li-ion Battery & it's working principle: ..... 11
2.4 Shape of Li-ion Battery ..... 13
2.4.1 Cylindrical Cells: ..... 13
2.4.2 Button Cells: ..... 13
2.4.3 Prismatic Cells: ..... 13
2.4.4 Pouch Cells: ..... 14
2.5 Parts of Li-ion Battery ..... 14
2.5.1 Anode ..... 14
2.5.1.1 Anode materials ..... 15
2.5.2 Separator ..... 15
2.5.3 Cathode ..... 16
2.5.4 Electrolyte ..... 17
2.5.5 Current Collectors ..... 18
2.6 Design Parameters of Li-ion battery: ..... 18
2.7 Structure of 18650 Li-ion Battery: ..... 19
2.8 The Pseudo-2-Dimensional (P2D) model: ..... 20
2.9 Temperature effect on LIBs ..... 21
2.10 Heat Generation in Li ion Battery ..... 22
Chapter 3 ..... 23
3.1 Research Methodology ..... 23
3.2 Experimental data analysis ..... 24
3.3 Simulation Procedure ..... 24

Chapter 4 ..... 27
Model development ..... 27
4.1 Cell Design ..... 27
4.1.1 1D Cell Design ..... 27
4.1.2 2D Cell Design ..... 27
4.1.3 3D Cell Design ..... 29
4.2 Cell Information ..... 30
4.3 Modelling of Lithium-ion Battery ..... 32
4.3.1. Electrochemical Modelling ..... 32
4.3.2 Thermal Modelling ..... 36
4.3.3 Electrochemical-Thermal Model coupling ..... 39
Chapter 5 ..... 41
Result & Discussion ..... 41
5.1 Model Validation ..... 41
5.1.1 Evolutions of the cell potential ..... 41
5.1.2 Evolutions of the cell temperature ..... 43
5.2 Effect of adding electrolyte channel ..... 45
5.2.1 Effect of Channel Width ..... 45
5.3 Effect of Channel Thickness ..... 49
5.4 Effect of Channel number ..... 52
Chapter 6 ..... 55
Conclusion ..... 55
Recommendations and future work ..... 57
List of References ..... 58

## List of Figures

Figure 1.1: Energy density for different rechargeable batteries[5] ..... 2

Figure 1.2 structure of a catheter located in the xylem of a trunk [35]..... 5

Figure 2.1:Operating mechanism of LIBs. [37] ..... 12

Figure 2.2 Battery cell configuration types: coin, cylindrical, prismatic, and pouch [38]..... 14

Figure 2.3 Comparative analysis of different cathode materials [44]..... 17

Figure 2.4 Design parameters for battery component ..... 19

Figure 2. 5 internal structure of 18650 li ion battery [49] ..... 20

Figure 2.6 Representation of the various kinds and processes of heat production in LIBs..... 22

Figure 3.1 Flow diagram of the research procedure..... 23

Figure 4.1 1D Cell Design..... 27

Figure 4.2 2D Cell Design: (a) Standard cell (b) Channel in negative electrode (c) Channel in positive electrode (d)Channel in both electrodes (e) The electrolyte channel's design was influenced by the structure of a catheter, which assists in the transportation of nutrients through the xylem of a trunk [35]. ..... 28

Figure 4.3 Model of 18650 Battery (a) Isometric view (b) Front view with dimension (c) Flow Compartment ..... 30

Figure 4.4 Schematic of a P2D lithium-ion battery model [64]..... 33

Figure 4.5 Electrochemical-Thermal coupling model..... 40

Figure 5.1 Comparison between an experiment and simulation at a different discharge rate of (a) Voltage (v) vs Capacity (Ah) (b) error(mv) between an experiment and simulation at a different discharge rate..... 42

Figure 5.2: Comparison between an experiment and simulation at a different discharge rate of (a) Temperature (v) vs time (s), (b) error(K) between an experiment and simulation at a different discharge rate..... 44

Figure 5.3 Temperature contour of the standard 18650 LFP cell at the end of 1C,2C,3C discharge ..... 45

Figure 5.4 The performance of adding electrolyte channel width for (a), (c), (e) temperature difference (K) and (b), (d), (f) capacity (Ah) ..... 47

Figure 5.5 Temperature contour of the 18650 LFP cell at the end of 3C discharge with various electrolyte channel widths from 10nm to 100nm: (a) both electrodes, (b) positive electrode, (c) negative electrode..... 48

Figure 5.6 The performance of adding electrolyte channel thickness for (a), (c), (e) temperature difference (K) and (b), (d), (f) capacity (Ah) difference ..... 50

Figure 5.7 Temperature contour of the 18650 LFP cell at the conclusion of a 3C discharge with various electrolyte channel thicknesses from 1 µm to 10 µm: (a) both electrodes, (b) positive electrode, (c) negative electrode. ..... 51

Figure 5.8 The performance of adding electrolyte channel number for (a), (c), (e) temperature difference (K) and (b), (d), (f) capacity (Ah) variations..... 53

Figure 5. 9 Temperature contour of the 18650 LFP cell at the end of a 3C discharge with various electrolyte channel numbers from 1 to 8: (a) both electrodes, (b) positive electrode, (c) negative electrode..... 54

## List of Tables

Table 1: 18650 Battery Specifications[48] ..... 20

Table 2: List of Model Parameters [32][48][62] ..... 31

Table 3:Thermal property parameters for each material of the battery. ..... 38

## Notation

| | |
|---|---|
| L | Electrode thickness |
| r | Radius |
| h | Battery height |
| k | reaction rate constant |
| C | concentration of lithium |
| σ | conductivity of the electrode |
| ε | volume fraction of a phase |
| D | diffusion coefficient |
| E | Activation energy |
| T | Temperature |
| F | Faraday constant |
| R | Ideal gas constant |
| t | time |
| j | reaction current density |
| $t^+$ | transference number |
| u | air velocity (m/s) |
| P | pressure (Pa) |
| μ | dynamic viscosity (Pa.s) |
| ρ | density ($kg/m^3$) |

Subscripts

| | |
|---|---|
| i | different layer of active material |
| p | Positive electrode |
| n | Negative electrode |
| sep | Separator |
| s | Solid |
| l | Liquid |
| D | diffusion coefficient |
| E | Activation energy |

| | |
|---|---|
| T | Temperature |
| F | Faraday constant |
| R | Ideal gas constant |
| K | Kinetics |
| d | diffusion |
| eq | open circuit potential |
| eff | Effective |
| ref | reference |

Superscripts

| | |
|---|---|
| 0 | Initial |
| max | maximum |
| surf | surface |

## Abbreviations

| | |
|---|---|
| SoC | State of current |
| SEI | Solid Electrolyte interface |
| LIBs | Lithium-ion battery |
| LFP | Lithium Iron Phosphate |

# Chapter 1

## Introduction

### 1.1 Background

Global warming has become one of the most important topics of discussion and concern worldwide. The impacts of climate change elicited by global warming are being reported widely in print and electronic media and are being researched extensively. Greenhouse gas emissions are a significant source of the global warming observed today[1]. Burning of fossil fuels is attributed to high levels of GHG emissions (accounting for about 75% of total emissions) and carbon dioxide emissions (at about 90%) [2]. The transition to renewable energy sources has been widely noted worldwide, becoming more critical because of climate change. These effects include extreme weather, increasing temperatures worldwide, and the most severe ecological shocks brought on by the greenhouse effect from fossil fuel emissions[3]. To address these challenges, renewable technologies like solar and wind energy are finding their place as a way of cutting down $CO_2$ emissions and moving towards carbon-less energy sources. A significant drawback of renewable energy sources is their intermittency, a problem even though they offer solutions to environmental issues. Solar and wind energy generation depends on weather conditions, time of day, and season, and hence cannot be easily integrated into the existing power system. Therefore, the demand for storage technologies has become more critical in the present energy systems.[4]. These systems facilitate the equilibrium of energy supply and demand by capturing surplus energy when production is elevated and discharging it during periods of deficiency. Lithium-ion (Li-ion) batteries are the most widely used technology for energy storage because of their high energy density, long cycle life, and low self-discharge rate. They are the central technology enabling the progress of sustainable energy systems, which are used in portable electronics, EVs, and large-scale energy storage for power networks and renewable integration[5].

The use of electric vehicles and renewable energy resources is rising worldwide, raising the demand for robust and effective energy storage systems. The lithium-ion (Li-ion) battery has unique inherent properties, making it the best candidate for many electrical storage applications. This success is because it is located at the highest point of the Ragone plot, as shown in Figure 1.1. Rechargeable batteries with higher power density and exciting energy density than other rechargeable batteries are Li-ion batteries[6]. Li-ion batteries also have good electrochemical and thermal stability, long battery life, low self-discharge rate, rapid charging-discharging capability, no memory effect, and no need for Maintenance. Because of their low self-discharge rates, long cycle life, and high energy density, lithium-ion (Li-ion) batteries are now the most widely used rechargeable batteries[7].

The fundamentals of electrochemistry underline how Li-ion batteries function. An electrolyte moves lithium ions between an anode and a cathode. Because it is necessary to charge and discharge the battery, this movement allows one to store and release energy. However, in these operations, heat is produced by electrochemical reactions, polarization, and the resistance of the battery's components. These systems naturally generate some heat, but if not controlled, this can lead to several issues with battery quality, durability, and safety[8]. It is also evident that thermal management is crucial because excessive internal temperatures in batteries can lead to several problems, such as a reduction in energy capacity, the decomposition of the battery's electrochemical components, such as the electrolyte and

electrodes, and even the possibility of thermal runaway, in which the temperature rises to the point where the battery explodes or catches fire. Hence, one of the most critical challenges in Li-ion batteries is the thermal management problem that affects battery performance, safety, and energy efficiency.[9].

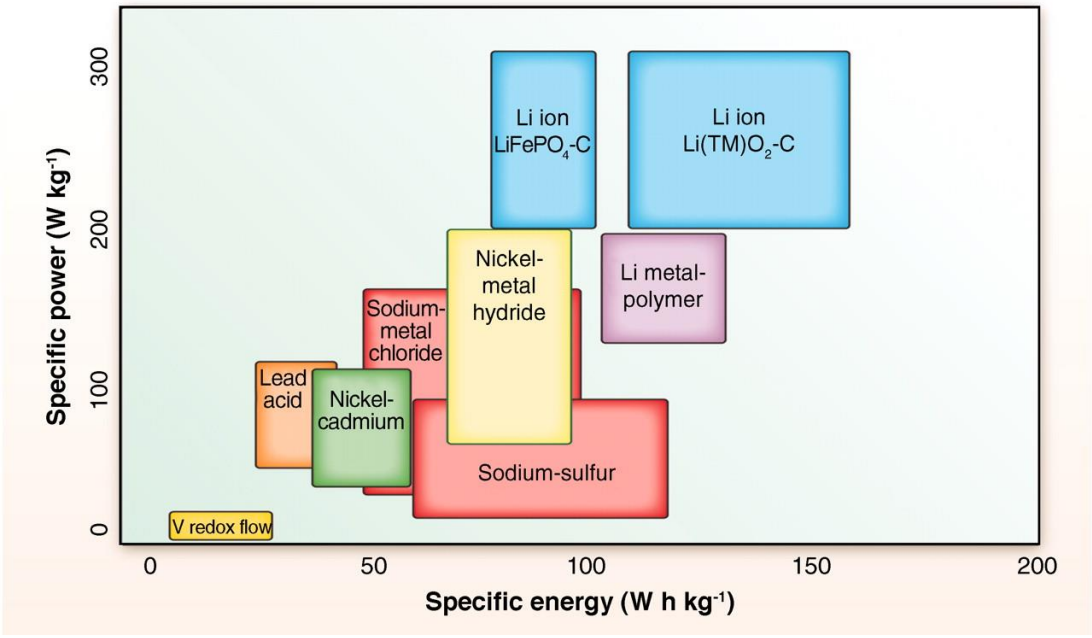


*Figure 1.1:* Energy density for different rechargeable batteries[5]

Lithium batteries are manufactured in various shapes and sizes depending on the application. These include cylindrical, prismatic, and pouch cells. Among these, cylindrical cells are one of the most widely used formats, particularly in applications where thermal management and cost efficiency are critical[10]. Cylindrical cells such as 18650 and 21700 are popular mainly due to their strong construction and balanced heat distribution [11]. However, larger cylindrical cells, like Tesla's 4680, have a problem with heat dissipation because of a lower surface area to volume ratio, which requires internal heat management systems[12]. Prismatic cells are rectangular-shaped and pack more cells per volume than cylindrical cells but have a non-uniform current flow that causes thermal hotspots, making cooling critical[13]. Pouch cells, which have flexible and lightweight constructions, can provide high energy density but have problems with swelling and unbalanced heat dissipation[14]. Both types depend on new materials and internal structures, such as stable electrolytes, high-conductivity additives, and electrode structures better designed to keep heat under control and ensure safety and performance in various situations.

Several electro-thermal models of lithium-ion batteries have been presented in published literature. It has been found that the thickness and the porosity of the electrodes play a significant role in the electrochemical performance of Li-ion batteries (LiBs), which in turn affects many other parameters such as power density, energy density, capacity loss, diffusion limitations, lithium plating, and lithium-ion deposition. Appiah et al.[15] analyze the influence of cathode thickness and porosity on Li-ion transport in LiNiO.6CoO.2MnO.2$O_2$/graphite, show that cathode thickness and porosity significantly

impact Li-ion cell energy and discharge performance with low-porosity cathodes suited for low-rate applications. Sing et al. [16] demonstrated that electrode thickness enhances the volume of the active material, subsequently improving the battery's energy density. This enhancement is relevant to applications like electric vehicles and large-scale energy storage systems that demand enduring power supply. However, electrode thickness presents significant challenges, such as capacity loss and diminished power density [17], [18]. Higher-porosity electrode materials can improve ion transport by increasing surface area [19]and making it easier for electrolytes to get into the material. This lowers polarization and improves electrochemical performance[20]. However, too much porosity reduces volumetric energy density, mechanical strength, and thermal conductivity. Optimized porosity reduces internal resistance and diffuses restrictions in thicker electrodes [21] also impacts thermal management since inadequate heat dissipation can result in thermal instability when energy demands are high.

While electrodes have more active material, they also have longer paths for ions to travel, which can cause polarization and lower capacity at high discharge rates. Improving transport and decreasing internal resistance through optimal porosity might improve these problems; nevertheless, mechanical strength and volumetric energy density are also negatively affected by excessive porosity[22]. Electrode thickness and well-designed porosity may reduce lithium plating during low-temperature or fast-charging operations, and it can transport and deposit ions uniformly while maintaining a balance between power and energy density[23].

Several works have been done on Li-ion battery's thermal performance, including analytical and numerical modeling, address temperature estimations, and lithium-ion battery cell prediction[10], [24], [25], [26], [27]. Heat in Li-ion batteries arises from three fundamental sources: ohmic heat, polarization heat caused by concentration gradients of lithium ions, and heat generated during electrochemical reactions. With inadequate thermal management, these elements would cause internal stresses, hot spots, and lithium dendrites, making it more challenging to prevent thermal runaway. In this case, electrodes offer significant benefits as they supply more active material for lithium storage, making them ideal for applications in electric vehicles and grid storage. This leads to extended diffusion paths for ions, raising internal resistance, polarization, and heat generation. The accumulation of heat results in the formation of gradients within the battery, impacting its operation and safety.

Moreover, thicker electrodes exhibit decreased thermal conductivity, exacerbating the issue of heat accumulation[22]. The greater the electrode thickness, the less the material can transmit heat and the more difficult it is to disperse the heat produced during operation. Because of this, the electrode gets hot spots in some places, which makes the temperature uneven and could damage the internal parts. The usage of batteries in high rate charging and discharging applications, where fast ion movement produces a lot of heat, makes this particularly problematic. Therefore, thicker electrodes offer a more significant energy density but also need more sophisticated thermal control systems to ensure safe operation. However, in terms of electrochemical performance and thermal management, thinner electrodes provide several benefits[28]. The shorter distance ions must travel between the anode and cathode causes them to have less internal resistance and produce less heat, allowing them to diffuse more quickly than fewer ions. Thinner electrodes are generally better at dissipating heat because they exhibit lower internal resistance and better thermal conductivity. This improved thermal

behaviour reduces the risk of overheating, creating a more stable environment for the electrochemical reactions. Therefore, thinner electrodes are suitable for applications that require high power density and short charge-discharge time, such as electric vehicles, where energy release and storage are critical. However, the trade-off is that thinner electrodes have lower energy capacity, which limits their use in applications that require long-duration energy storage[29].

One of the most popular cylindrical formats is the 18650 cells, often used in portable electronics, power tools, and electric vehicles. The 18650 batteries, with their standard dimensions of 18mm in diameter and 65mm in length, are favoured for their high energy density, excellent thermal management, and long cycle life [30]. The rapid usage of 18650 Li-ion batteries in a variety of applications, ranging from consumer electronics to electric cars, may be attributed to the desire for energy storage systems that are high-performing, reliable, and safe[11]. Temperature behaviour is a crucial aspect affecting these batteries' efficiency, safety, and longevity. Understanding how electrode structure affects thermal behaviour is critical for optimizing battery design and enhancing thermal management strategies[31]. 18650 cells are particularly prevalent in electric vehicle battery packs, notably in Tesla vehicles, where large arrays provide the necessary power density and capacity for long-range driving. The widespread use of 18650 cells is mainly due to their robustness, reliability, and ease of manufacture, combined with the high degree of standardization they offer for mass production[9].

Various 18650 batteries are available, each with its unique chemical composition (LFP, LMO, NMC, etc.). These batteries are employed in many applications, starting from tiny appliances for home use, automobiles such as electric cars, and heavy-duty power tools, and differ in energy density, capacity, discharge rates, and safety features [32]. Thermal management is especially critical for 18650 cylindrical cells, mainly in high-power applications like electric vehicles, where rapid charge-discharge cycles can lead to significant heat buildup. As the energy density of these cells increases, the heat dissipation capacity becomes a limiting factor. Saw et al. [33] analyse thermal behaviours in 18650 $LiFePO_4$ cells using a coupled P2D and thermal model, emphasizing the impact of heat generation and electrical resistance on temperature gradients during fast charging. Excessive heat can cause thermal degradation of the cell materials, reduce battery efficiency, and, in extreme cases, lead to thermal runaway. Excessive heat generation and accumulation within the battery can degrade performance, shorten lifespan, and even offer safety issues like thermal runaway and fires, making thermal management critical[34].

Innovative electrode designs are crucial for addressing lithium-ion batteries' electrochemical and thermal challenges. One notable advancement is the addition of electrolyte channels. Gao et al. [35] present a bio-inspired design of electrolyte channels that significantly improve the performance of lithium-ion batteries. This innovation enhances specific energy, capacity, and power by optimizing ion flow and reducing mechanical stress during fast charging. Compared to traditional cells, this channel design approach can enhance specific energy by up to 79% and may reduce the danger of lithium plating, making it promise. Patel et al.[36] demonstrated that lithium-ion battery electrodes, including electrolyte channels in thick electrodes, increase ion transport, mitigate the dangers of lithium plating, and improve high C-rate performance, although with a minor reduction in low capacity and energy density due to reduced active material. These channels enhance realized capacity at higher discharge rates, particularly on the anode side, by improving access to active materials. However, their effect on

plating is inconsistent; they reduce plating risk when used on the anode alone, but they don't do much more when applied to both electrodes.

## 1.2 Problem Statement

The rise in temperature during operation significantly impacts the performance of Lithium-ion (Li-ion) batteries, which are essential components in modern energy storage systems. This temperature increases results from several factors, including internal resistance, heat generated by electrochemical reactions, and energy losses during charging and discharging. The ensuing thermal buildup compromises battery efficiency and accelerates degradation, shortening the battery's lifespan. More critically, this temperature rise poses substantial safety risks, such as overheating and thermal runaway, which can have severe consequences. Despite extensive research to mitigate these issues, the effective control and reduction of temperature rise remain a persistent and challenging problem in developing safer, longer-lasting Li-ion batteries.

### 1.3 Motivation of this study

The motivation for designing an electrode with an added electrolyte channel comes from the bio-inspired catheter structure in the xylem of a trunk shown in Figure 1.2. This idea was proposed by Gao et al. [35]. This design concept ensures a more efficient delivery of nutrients to the tree's crown through the catheter. The electrolyte channels in the electrodes enhance the cell's performance by increasing the movement of lithium ions. Increasing contact area can increase ionic conductivity, transport more ions, and reduce internal resistance for fast discharging/charging; this could theoretically enhance thermal performance.

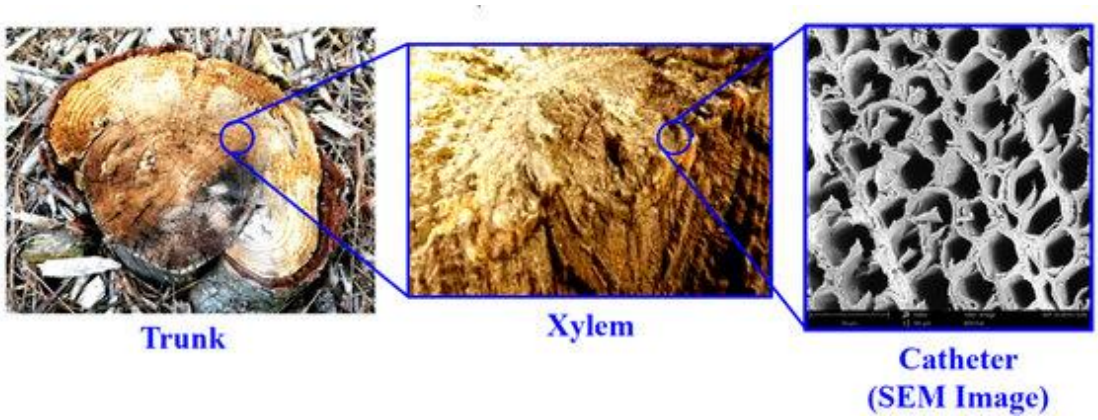


Figure 1.2 structure of a catheter located in the xylem of a trunk [35]

### 1.4 Objectives of this study:

This study aims to minimize internal heat generation in Li-ion cells by modifying electrode design using physics-based modelling. The following objectives assist in accomplishing this goal:

1. To modify the electrode surface by creating electrolyte channels to reduce excess heat generation in lithium-ion cells via physics-based modelling.
2. Design a thermal model of 18650 Li-ion batteries with different configurations of electrode channels modified based on physics-based modelling.
3. To investigate and predict the thermal response of the battery for different design scenarios of the electrolyte channel in the electrode structure.
4. to determine the optimum channel incorporated electrode design parameter for less heat generation

## 1.4 Thesis Outline

This thesis consists of Six chapters.

**Chapter 1:** overviews the background and introductory information on the identified problem. It also discusses relevant literature reviews, the objectives of this study, and the research questions.

**Chapter 2:** Theories that are needed for describing this topic is briefly discussed in this chapter

**Chapter 3:** Research methodology of this simulation procedure described in this chapter

**Chapter 4:** Mathematical model, Model development, design model, and simulation procedure are described in chapter

**Chapter 5:** Results & discussion of this study illustrated in this chapter

**Chapter 6:** The conclusion and recommendations given in this chapter

# Chapter 2

## Theory

### 2.1 Electrochemical Cells

Alessandro Volta first described the current generation process as an electrochemical reaction of different metals separated by an ion-conduction and an acidic medium. Electrochemical cells can be divided into batteries, capacitors, and fuel cells. Capacitors can provide a high amount of energy for a short period of time, while fuel cells can produce electric energy from the reaction of hydrolysis occurring between oxygen and hydrogen; this reaction does not involve fossil fuels; the only product is water.

#### 2.1.1 Battery

A battery is an object or component on which optional electrical energy can be delivered and obtained by converting chemical energy. This comprises one or more electrochemical cells, each containing a cathode, an anode, an electrolyte, and a separator. Battery storage devices, ranging from small handheld devices to large vehicles, are critical in society's current technology. The conversion process occurs during an electrochemical oxidation-reduction (redox) reaction, that is, the transfer of electrons from the oxidized electrode to the reduced electrode.

$$\text{Reduction: } \mathrm{A}^{n+} + \mathrm{ne}^{-} \longrightarrow \mathrm{A} \tag{1}$$

$$\text{Oxidation: } \mathrm{A}^{n-} \longrightarrow \mathrm{A} + \mathrm{ne}^{-} \tag{2}$$

#### 2.1.2 Types of Battery

##### 2.1.2.1 Primary Batteries:

Primary batteries are used only one time and cannot be recharged. These are non-rechargeable type of battery commonly found in kid's toys, remote controls and flashlights among others non-rechargeable batteries used in devices like toys, remote controls, and flashlights. Some of them are alkaline, zinc-carbon as well as lithium batteries.

##### 2.1.2.2 Secondary Batteries:

Secondary batteries are designed for using many cycles as charging discharging. In the early 21$^{st}$ century, secondary batteries becoming more famous and raising value into the global market. In general sense, these types of batteries are more economical than primary batteries but initially purchase cost higher then primary battery. These are rechargeable batteries used in applications like electric vehicles, backup power systems, and portable electronics. Examples include lead-acid, nickel-cadmium (NiCd), nickel-metal hydride (NiMH), and lithium-ion (Li-ion) batteries.

## 2.2 Battery terminology

### 2.2.1 Battery Capacity & power

Among the fundamental factors in determining the type of battery required is its power and capacity. The battery's capacity determines the system's function and the type of performance that will be achieved. It is measured in kilowatt-hours (kWh), units of stored energy, and ampere-hours (Ah), units of capacity. The most straightforward method of determining the battery's capacity is to cycle it until its self-discharges to the lowest voltage specified by the manufacturer. After two hours of charging the battery at a constant current (CC) regime, the charger reaches the maximum voltage in its maximum current mode. Subsequently, it is charged at a constant voltage (CV) until the current diminishes to 5% to 10% of its initial value. This charge method is referred to as CC/CV. The current is then integrated throughout the discharge duration to get the capacity. The charging and discharging power limit is the next important consideration. In any application, a battery must be able to deliver power whenever needed to achieve a suitable performance level. A battery's C-rate, or the rate at which it will discharge its total capacity in an hour, is determined by measuring the current about the battery's capacity. For instance, this translates to a current of 12A for a 12 Ah battery. It would discharge in two hours at 0.5C and 6A, but at 2C and 24A, it would discharge in half an hour. To prevent additional damage to the components, the battery voltage may occasionally be required to be maintained within the range advised by the instructions.

### 2.2.2 C-rate

The C-rate quantifies a battery's charging or discharging capability relative to its rated capacity. The calculation can be performed using equation 4, where rated capacity is expressed in ampere-hours and current in amperes. A rate of 1 C signifies charging or discharging the specified capacity in one hour, whereas a rate of 2 C indicates charging or discharging the rated capacity in thirty minutes. The lifetime, total capacity, and voltage parameters may be contingent upon the C-rate. This renders it a crucial parameter when analysing and comparing batteries.

$$C\ rate = \frac{Charge\ or\ discharge\ current(A)}{Nominal\ capacity\ (Ah)} \tag{3}$$

### 2.2.3 State of Health (SoH)

A critical characterization parameter of a battery is the state of health (SOH), which is relevant both during its operational lifespan and when evaluating its potential for second-use applications. This value indicates the degree of fullness of the present overall capacity relative to a specified anticipated capacity. As previously said, numerous methods can be employed to obtain an accurate estimation. Specific procedures are predominantly conducted in the laboratory due to the necessity for specialized and intricate equipment. These are primarily utilized whenever a status report is necessary before using the cart or for routine inspections. Assessing the internal resistance of a battery is a technique that indicates the aging and deterioration of its components. Usually, it is determined from the slope of the voltage drop across the battery on load divided by its no-load voltage, which is its open circuit voltage (OCV). They are supplied with varying pulse currents, and the output results for the tests are satisfactory. This method's main limitation is the relative time required by the battery to come to equilibrium to achieve the OCV reading. There is another method that encompasses the determination

of the impedance of that battery. This value is also directly linked to battery ageing. Impedance is often measured using electrochemical impedance spectroscopy, widely applied in the last decade to measure the impedance. This approach is responsive to minor frequency variation while providing more detailed information on primary areas of battery losses. If predictions of the State of Health (SOH) are needed without any measurements using such equipment or when battery pack dismantling is impossible, modelling methods or data history may be used. However, the approximate level of the remaining capacity can be arrived at by registering the number of cycles and worst-case scenarios related to power and output or temperature conditions during the battery's lifespan.

$$SoH = \frac{Rated\ Capacity}{Nominal\ Capacity} \tag{4}$$

### 2.2.4 State of Charge (SoC)

It is essential to ascertain the energy level of a battery at any given moment to facilitate optimal system design. The state of charge (SOC) can be computed using numerous approaches. The most straightforward method is dividing the existing voltage by the open circuit voltage, which is called OCV. While this type of relationship yields a nearly linear correlation for lead-acid batteries, it does not apply to lithium-ion batteries. Like SOH estimates, SOC can be assessed by impedance measurements; however, this method is limited to real-time estimation. Accounting methods are among the most prevalent in lithium-ion batteries for determining the state of charge (SOC). This encompasses the assessment of the residual depth of drain of the battery utilizing real-time current or power input or output from the battery. The state of charge (SOC) at any time step is contingent upon the SOC of the preceding time step, SOC(t-1), allowing for the determination of SOC(t) based on the instantaneous current, I(t), and notional capacity. This technique, called coulomb counting, is straightforward and widely employed for estimating the state of charge (SOC). The experimental data of the battery pack can be utilized to enhance the precision of SOC values and loss factors, including temperature, history, and cycle life. This also raises the accuracy of current estimates and improves SOC estimations. Additional methodologies, including neural networks, Kalman filters, and fuzzy logic, are also examined for state-of-charge estimation. These strategies are occasionally employed in conjunction to attain enhanced precision when the outcome is derived subsequently.

$$SoC = \frac{stored\ capacity}{Rated\ Capacity} \tag{5}$$

### 2.2.5 Depth of Charge (DoD)

The Depth of Charge (DoD) is opposite of SoC. It defines what percentage of capacity is used during discharge. For example, if a battery have 100Ah capacity and that is discharged by 30Ah so that DoD is 30% and Soc is 70%.

### 2.2.6 Open Circuit Voltage (OCV)

The open circuit voltage (OCV) is the voltage that results when the battery is not receiving or transmitting current, indicating that there are no reactions occurring within. Since OCV depends on

the battery's state-of-charge, it should not change over its useful life. However, other aspects of batteries vary with time; for example, capacity decreases with time due to charge-discharge cycles.

### 2.2.7 Terminal Voltage (V)

A determination of the voltage across the battery terminals in relation to the supply current. The terminal voltage depends on power output and discharge/charge current. The potential or voltage at the battery's terminals separates the anode and cathode. The theoretical terminal open circuit potential is given by the difference between the two electric metals when the electrodes are separated from the circuit. The electrochemical series is where the materials' potential is. The standard operating procedure for describing a material's capacity is placing one material on the zero-dimensional axis and the second along the positive or negative axis. The difference in the hydrogen capacity is then measured. Due to the low potential of Li/Li+, an alternative scale is occasionally employed in which Li/Li+ is set to zero. This scale is seldom found on the left side of the scale.

### 2.2.8 Nominal Voltage (V)

The voltage of the battery that is recorded or used as a reference of the battery, which is also sometimes considered to be the "normal" voltage of the battery. This voltage is also sometimes referred to as the charge voltage.

### 2.2.9 Cut-off Voltage (V)

It is the minimum tolerable voltage. The "empty" state of the battery is generally characterized by this voltage, which represents the current voltage level.

### 2.2.10 Energy or Nominal Energy (Wh)

The total Watt-hours of energy discharge capacity of the battery when the battery is discharged under a specific current strength (expressed by a C-rate) starting from the fully charged state down to a resting voltage. Energy is estimated by multiplying the discharge power by the unit of discharge time as a watt-hour. As with capacity, energy also gradually deteriorates with the increase of C-rate.

### 2.2.11 Specific Energy (Wh/kg)

Specifically, the energy of a battery is expressed in terms of its nominal energy per unit mass, which is denoted by the symbol Wh/kg. It is highly dependent on the chemistry of the battery as well as the packaging.

$$\text{Specific Energy}\left(\frac{\text{Wh}}{\text{kg}}\right) = \frac{Nominal\ voltage\ in\ Volts\ (V) \times battery\ capacity\ (Ah)}{mass\ of\ the\ battery\ (m)} \qquad (6)$$

### 2.2.12 Specific Power (W/kg)

Therefore, the specific power of a battery can be presented in several distinguishable units, such as watts per kilogram, watt-hours per kilogram, W/kg, WH/kg, and kW/kg. We are more sensitive to the chemistry of the battery and specifically to the packaging when it comes to this than to the first two.

$$Speciic\ Power\ \left(\frac{W}{kg}\right) = \frac{Maximum\ Power\ Output\ (W)}{Mass\ of\ the\ Battery\ (kg)} \quad (7)$$

### 2.2.13 Energy Density (Wh/L)

Energy density of lithium-ion batteries (LIBs) can be expressed in two main forms: gravimetric energy density (energy per unit mass) and volumetric energy density (energy per unit volume).

$$Volumetric\ Energy\ Density = \frac{Energy\ (Wh)}{Volume\ (L)} \quad (8)$$

$$Gravimetric\ Energy\ Density\ = \frac{Energy\ (Wh)}{Mass\ of\ the\ Battery\ (kg)} \quad (9)$$

### 2.2.14 Power Density (W/L)

Power density of battery measures capability of a battery to deliver power per unit of volume or mass. It is commonly expressed in units of W/L (volumetric power density) or kW/L, and sometimes in W/kg (gravimetric power density).

$$GravimetricPower\ Density\ = \frac{Power\ (W)}{Mass\ of\ the\ Battery\ (kg)} \quad (10)$$

$$Volumetric\ Power\ Density = \frac{\text{Power}\ (W)}{Volume\ (L)} \quad (11)$$

## 2.3 Li-ion Battery & it's working principle:

A Li-ion battery cell consists of several essential components: an anode, a cathode, a central separator, and current collectors arranged on the two sides of the anode and cathode, respectively. The name Li-ion battery cell is obtained from the cathode material, which is a composite material. The anode material is usually made from graphite or a metal oxide. Three different types of electrolytes can be classified as solid, liquid or polymer. The separator is made to be permeable to allow the movement of lithium ions while at the same time acting as a barrier to thermal runaway and short-circuiting within the cell. The cathode and anode exhibit varying electrode potentials to cause the flow of electric current through the external circuit to drive the load. During the charging process, an opposite effect occurs. The lithium ions will be released from the cathode and move to the anode due to the current passing through the cell. Intercalation, the process of charging the battery, occurs at the battery's anode. A brief description of the operating mechanism of the Li-ion battery is shown in Figure 2.1 below.

In a lithium-ion battery, the charging and discharging operations include the movement of lithium ions between the electrodes. This movement is the fundamental working principle of the battery. While charging, lithium ions move between the positive and negative electrodes, intercalating into the former and de-intercalating from the latter. The positive electrode releases electrons, which move to the negative electrode via the external circuit at the same time. While discharge is taking place, the flow of electrons from the negative electrode to the positive electrode via the external circuit is in the opposite direction of the flow of lithium ions back to the positive electrode. Heat is produced within the cell because of these processes, and it is then dissipated in every direction across the cell. The electrochemical reactions that control these processes are described by the following equations.

**Negative electrode:**

$$LiC_6 \underset{Discharge}{\overset{Charge}{\leftrightarrows}} C_6 + xLi^+ + xe^- \quad (12)$$

**Positive electrode:**

$$LiFePO_4 \underset{Discharge}{\overset{Charge}{\leftrightarrows}} xLi + xe- + Li_{1-x}FePO_4 \quad (13)$$

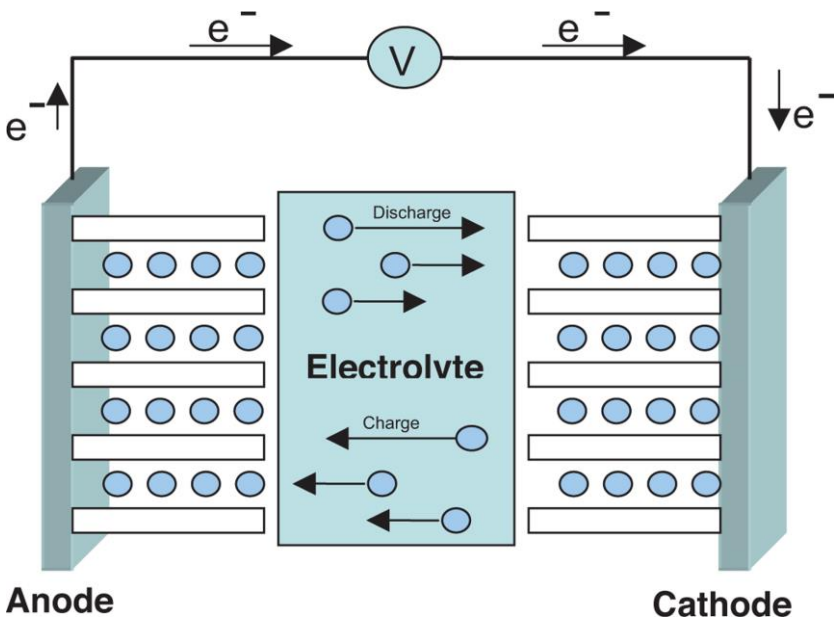


Figure 2.1:Operating mechanism of LIBs. [37]

## 2.4 Shape of Li-ion Battery

### 2.4.1 Cylindrical Cells:

Lithium-ion cylindrical batteries are common types of batteries characterized by straightforward structure and manufacturing process. This has led to their versatility in laptops, electric vehicles, and many other applications. The internal structure of these batteries is generally a 'jelly roll' arrangement of the anode, cathode and separator in a cylindrical construction. Cylindrical cell capacity is directly related to dimensions and, most importantly, to the diameter—thicker cells offer better capacity due to the greater internal surface area. For example, the 18650 cells largest dimension is 18mm diameter and 65mm height; on the other hand, 21700 has a dimension of 21mm diameter and 70mm height, which represents a higher capacity. The main strength of adopting this cell format is that it is easily manufacturable and cost-effective. However, there are some issues, such as thermal problems and difficulties in the system's packaging system's packaging. The cylindrical cells are prone to heat during high-power application and thus need proper coolants to enhance their performance and longevity. In addition, packing the cells in devices in a cylindrical manner may also be inefficient since the gaps between them decrease the energy density of the pack. Nevertheless, cylindrical cells are widely used in the industry with different capacities for consumer electronics, electric vehicles, and even power tools devices; various kinds of cylindrical batteries are available, including AAA, AA, C, and D batteries, which clearly illustrate the applicability of this form factor. The design is cost-effective and efficient in performance with the added advantage of being easy to manufacture and thus commonly used in various technological devices.

### 2.4.2 Button Cells:

A button cell, or coin cell, is a small, round battery used in devices like watches, calculators, and hearing aids. Made of stainless steel, it has a flat positive terminal and a cylindrical negative terminal. Common chemistries include lithium (high energy density), silver oxide (precision in low-drain devices), and alkaline. Compact and long-lasting, button cells are ideal for miniaturized electronics but require careful handling due to safety and environmental concerns.

### 2.4.3 Prismatic Cells:

There are two main types of formation of prismatic cells, stacked or wound, depending on the cell values that need to be achieved. As for terminology, the format is defined in terms of thickness, width and depth. The only significant difference between prismatic and pouch cells is in the design of the casing, while the former boasts a hard casing of Aluminium. It is possible to construct high-density batteries based on prismatic cells, but the thermal issue of ion packaging may arise. Neighbouring cells may heat each other because of heat dissipation, so various thermal regulation parts are located between the pack's cells. These flat, rectangular batteries are used in applications requiring higher energy density and specific form factors, such as in smartphones (e.g., Samsung Galaxy S series) and laptops. Different types of cell configurations shown in *Figure 2.2*.

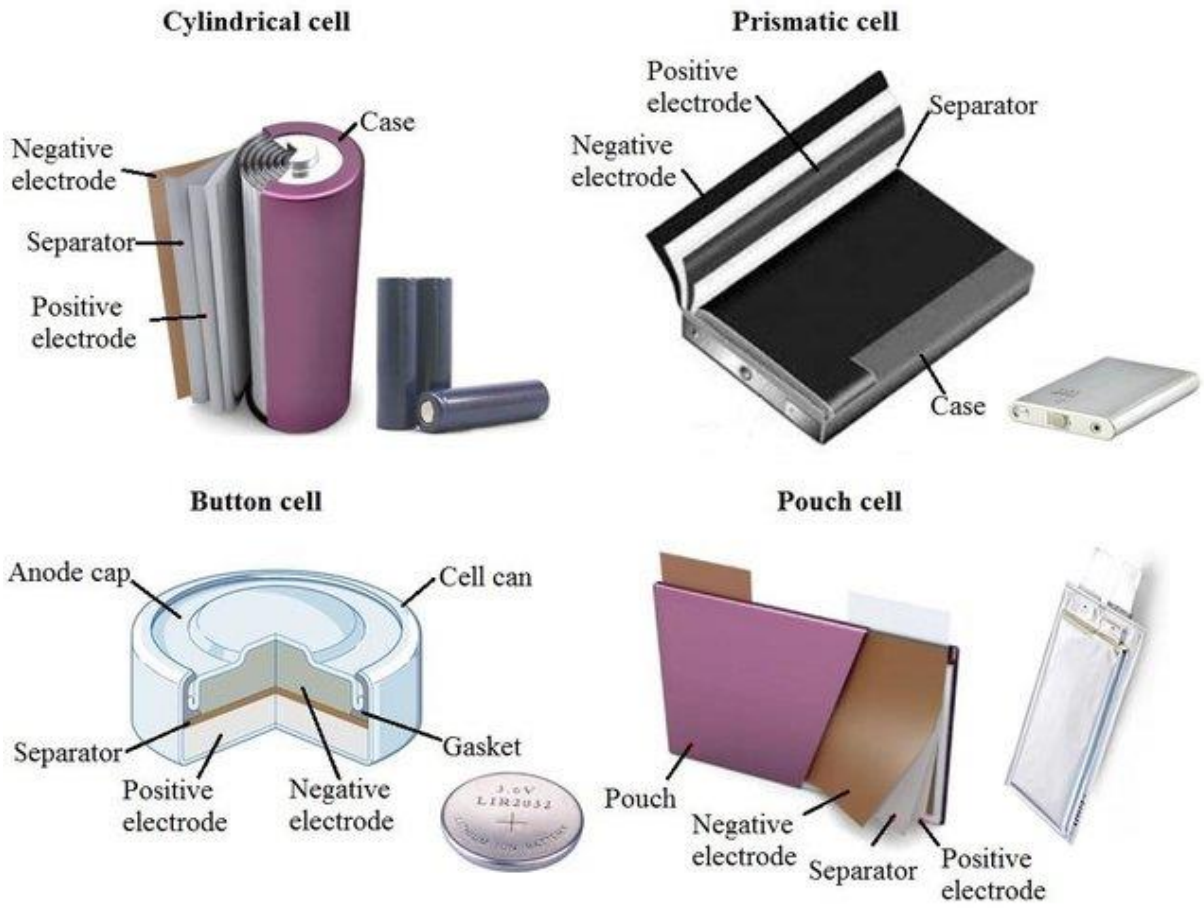


Figure 2.2 Battery cell configuration types: coin, cylindrical, prismatic, and pouch [38]

### 2.4.4 Pouch Cells:

Prismatic or flat in the basic format, pouch cells are encapsulated in a soft package casing, most common made of polymer-laminated aluminium foil, and its electrodes are typically stacked or Z-folded, depending on the capacity of the cell and other operation characteristics. Heat or ultrasonic welding are utilized in the package sealing. Like what happens with prismatic cells, thermal management devices are placed between the cells in a pack, to ensure a safe operation. These flexible, pouch-shaped batteries are used in applications where space and weight are critical, such as in wearable devices (e.g., Apple Watch) and medical implants.

## 2.5 Parts of Li-ion Battery

### 2.5.1 Anode

Carbonaceous materials are the most common type of anode material. Anodes, like cathodes, must be structurally stable enough to contain large amounts of lithium without significantly changing their properties; they must also be inexpensive, good electrical and ionic conductors, and chemically and electrochemically stable with the electrolyte.

#### 2.5.1.1 Anode materials

Lithium metal, with the highest specific capacity, was noticed as an anode material during the 1970s and early 1980s. However, it was confronted with some drawbacks that limited its efficiency, mainly the problem of lithium dendrites formation during charging. These dendrites could grow out of the anode, thus encountering the second electrode, leaving behind “dead lithium” against the anode or in the electrolyte solution during discharge. This process consumed active material and decreased the battery’s cycle life and safety. However, developing a solid electrolyte interface layer on the lithium anode introduced other problems, such as self-discharge, high kinetic impediments, cycling efficiency and capacity decay. Consequently, researchers found themselves looking for different types of anode materials to avoid these problems.[39]

The high applicability of lithium-ion batteries is due to the transition from lithium metal to lithium-containing compounds in the anode while enhancing safety and performance. Graphitic carbon was selected among the primary materials chosen as it has a high-reliability coefficient and is not toxic. Apart from that, graphitic carbon is cheap compared to other materials. Carbon-based materials have been crucial to the rapid development and commercialization of lithium-ion batteries, with several key advantages: They are inexpensive, increase safety and have a bare insertion potential of about 0.1V compared to Li/Li+ potential. These materials also boast high mechanical strength, which can explain high cycling stability even after 500 charge-discharge cycles, and their theoretical capacity is higher than that of transition metal oxides or sulphides[40].

One of the most essential carbon features in lithium-ion batteries is the ability of intercalation, which means lithium ions are being inserted in the layered structure of carbon without adversely affecting the structure. In discharging, lithium ions go to the carbon interior, and during charging, they are released back into the electrolyte. Carbon is the fourth element in the periodic system, and it is present in various qualities whose structures vary according to their application, preparation, and source. Soft carbon, stiff carbon and graphite are the three most popular forms of carbon used in lithium-ion batteries. In the mid-1990s, Sony faced the problem of propylene carbonate co-intercalation and thus used coke as an anode material. This development saw more use of graphitic mesophase microbeads (MCMBs), which seem to have a capacity of about 300 mAh/g and relatively low irreversible capacity. Although graphite possesses a theoretical capacity of slightly over 372 mAh/g for $LiC_6$, it has problems of higher irreversible capacity and faster decay rates besides the above-mentioned ones in comparison with MCMBs. After that, the study was carried out intensely in high-capacity anode materials, whereas non-graphite anodes such as hard and soft carbons were also studied intensely.

### 2.5.2 Separator

In lithium-ion batteries, a separator prevents direct contact between the anode and the cathode while enabling the ions to pass through the two components. It is inserted in the form of a microporous film; however, it also contributes impendence and augments the total weight of the battery. Thus, the choice of the separator material can significantly affect the battery's performance and must be chosen correctly. Most commercial lithium-ion batteries are separated by polyolefin materials such as polyethene (PE) or polypropylene (PP). For these separators to be effective, they must meet certain specifications, as explained below. They must be robust enough to support automatic manufacturing and not shrink; they have to be durable to avoid punctures by the electrodes. It is preferable if the

separator has tiny pores, which should be less than one micron for harmonious ion movement. It should also be free to absorb the electrolyte where ions can effectively flow, particularly into the separator. Moreover, the separator must be chemically compatible with other constituents of the battery, the electrodes, and the electrolyte, the stability of which cannot degrade during the battery's lifetime[41].

Polyolefin separators are generally single-layer and may consist of polyethene or polypropylene and a polyethene/polypropylene blend. These materials usually have a pore size of 0.03 to 0.1µm; the separator media is about 30 - 50% pores[41]. In addition, the separator also has an essential capability for battery safety, mainly when the temperature is high. Its relatively low melting point makes polyethene a safeguard if the apparatus is overheated. As the temperature increases, the polyethene component softens, the separator shrinks, and the size of its through pores decreases; therefore, the rate of lithium ions' movement also decreases. If the temperature rises, the separator will shut down the circulation and protect the battery from getting hotter. For separators with both PE and PP in the composition, this occurs near 130 °C, about 165 °C, and the material completely turns to a liquid state and does not let fire through to the battery or result in failure.

### 2.5.3 Cathode

The cathodes in lithium-ion batteries are an intercalation compound that may comprise metal oxides such as lithium cobalt oxide, lithium iron phosphate, and manganese oxide [42]. These materials play a role in defining the function of the battery due to their ability to reversibly store and release lithium ions without undergoing a significant amount of change in platform structure. Also, the cathode material must be chemically and electrochemically stable with the electrolyte, have a good electric conductor, provide proper diffusivity of lithium ions and have a relatively low cost. The battery's thermal stability and rate capability depend on the cathode materials, hence having a president in overall battery performance. In the arrangement of *Figure 2.3* F, there is a comparison of the different kinds of cathode materials, including the advantages and disadvantages that each possesses.

Lithium Cobalt Oxide is the most common cathode material due to its good cycle life and high energy density. Lithium ions are inserted between layers of cobalt oxide, $CoO_2$, and have a theoretical energy density of 274/1000mAh/g [43]. However, the realizable capacity is generally below 140–160 mAh/g, caused by anisotropic structural transformations at the lithium concentration, $Li0.5CoO_2$. New coatings such as $AlPO_4$ have been applied to optimize capacity retention and thermal characteristics. $LiCoO_2$ also displays reasonable discharge capacity in which the cathode boosted by the CNTs multi-walled has delivered 136 mAh/g at the rate of 5C. However, cobalt is less abundant and more costly than other TM like Mn and Fe; as a result, $LiCoO_2$ is comparatively expensive despite its acceptable electrical conductivity. Lithium Manganese Oxide ($LiMn_2O_4$), LMO has a better outlook for its cubic spinel structure[43]. This material has an intrinsic specific capacity of about 148 mAh/g, and the current designs offer a reversible capacity of 115 – 130 mAh/g at a 1C rate or less. $LiMn_2O_4$ nanowire cathodes have presented a high-power property with 107 mAh/g at 5C, 102 mAh/g at 10C, and nearly no capacity fade after 100 cycles. It is found that when other transition metals such as nickel, cobalt, or iron are incorporated in $LiMn_2O_4$, the capacity and the capacity retention in cycling become even superior. This puts $LiMn_2O_4$ in a good position to be used when high power density and more extended energy storage are needed. $LiFePO_4$ (LFP), or Lithium Iron Phosphate, is comparatively new to the field of cathode materials. It has an olivine structure, which differs from the layered and spinel structures in

most Li-ion materials. The intercalation mechanism is, therefore, phase change. LFP has a theoretical specific capacity of 170 mAh/g, while recent development has made those figures more achievable. For instance, $LiFePO_4$ composites with a nano-carbon wire network present high capacity and high-rate capability during tests. They delivered 129 mAh/g at a 10C rate and more than 90% C-capacity retention after 400 cycles at a 10C rate. LFP can further be described as inexpensive and environmentally friendly, and the battery possesses high safety standards, making LFP suited for applications that require high cost and sustainability.

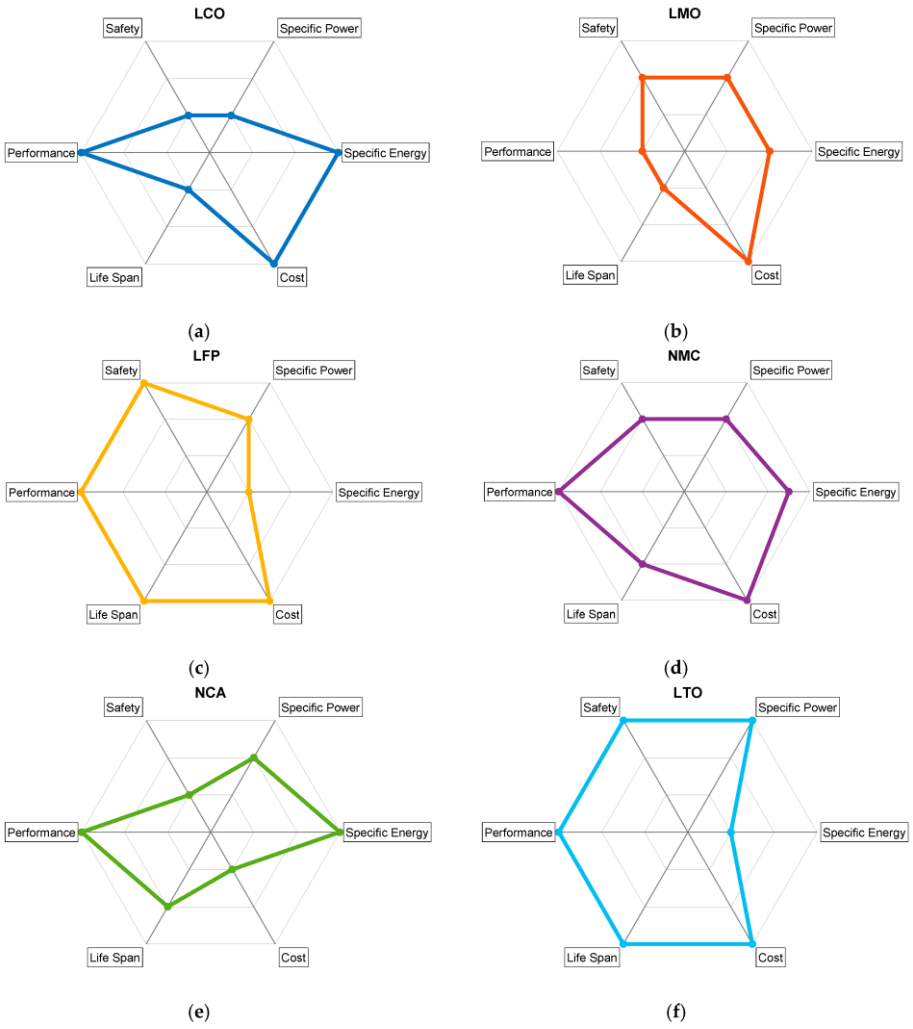


Figure 2.3 Comparative analysis of different cathode materials [44]

### 2.5.4 Electrolyte

A lithium-ion battery's electrolyte is vital for operation at high energy densities and maintaining safety. Lithium salt is usually dissolved in organic solvents. Some examples of ubiquitous solvents are alkyl carbonates, such as ethylene carbonate, and the lithium salt $LiPF_6$. Therefore, a suitable electrolyte must meet the following criteria: high ionic conductivity, low toxicity, an appropriate operation voltage range, which is 0V to 5V and thermal stability. $LiPF_6$ has been chosen as a standard because this solute exhibits the desired characteristics of both strength and conductivity [45].

Studies have also aimed at enhancing thermal stability because battery performance decays rapidly at temperatures above 60°C. New salts such as lithium Bis Borate (LiBOB) and blends of LiPF6 with other salts have been shown to possess better thermal stability up to temperatures of 80. Ionic liquids provide a high safety level because of flame-resistant and high ionic strength but are expensive and less efficient at high voltage. In this connection, new electrolytes are being designed to enhance future lithium-ion batteries' safety and thermal stability performance [45].

### 2.5.5 Current Collectors

Modern collectors comprise a battery that moves electrons from the electrodes to an external circuit. Several types of current collectors are available: mesh, foam, and foil. Thin and light foils are desirable to reduce the overall size and increase the volumetric density of the cells. Current collectors in today's LIBs have an electrochemically inactive volume in the cell but offer the surface to which the electrochemically active materials are applied. The active materials are deposited on the thin current collectors as a conducting agent and adhesive binder [46]. Therefore, current collectors should exhibit low cell resistance due to high electrical conductivity and chemical stability when in contact with a liquid electrolyte in the operating voltage range of active electrodes. This means that different current collectors can cause a big difference in the performance of lithium-ion batteries[47]. The 16 most utilized current collectors in commercial batteries are copper foil for the positive electrode (Cathode) and aluminium foil for the negative electrode (Anode).

## 2.6 Design Parameters of Li-ion battery:

The thickness, surface-to-volume ratio, cathode to anode area ratio, mass ratio, electrode density, particle size, porosity, tortuosity, and geometry and arrangement of the current collectors are the most essential geometric properties of a battery that determines its performance. The following factors have a particularly big impact on battery performance: thickness, electrode density, particle size, area ratio, mass ratio, and surface to volume ratio. Additionally, the energy potential is greatly influenced by the geometric properties of the electrolyte, current collectors, and separators. The usual characteristics of the lithium-ion battery components are shown in *Figure 2.4*. Other design factors related to the properties of the material, such as the separator, current density, and lithium-ion conductivity, are also included.

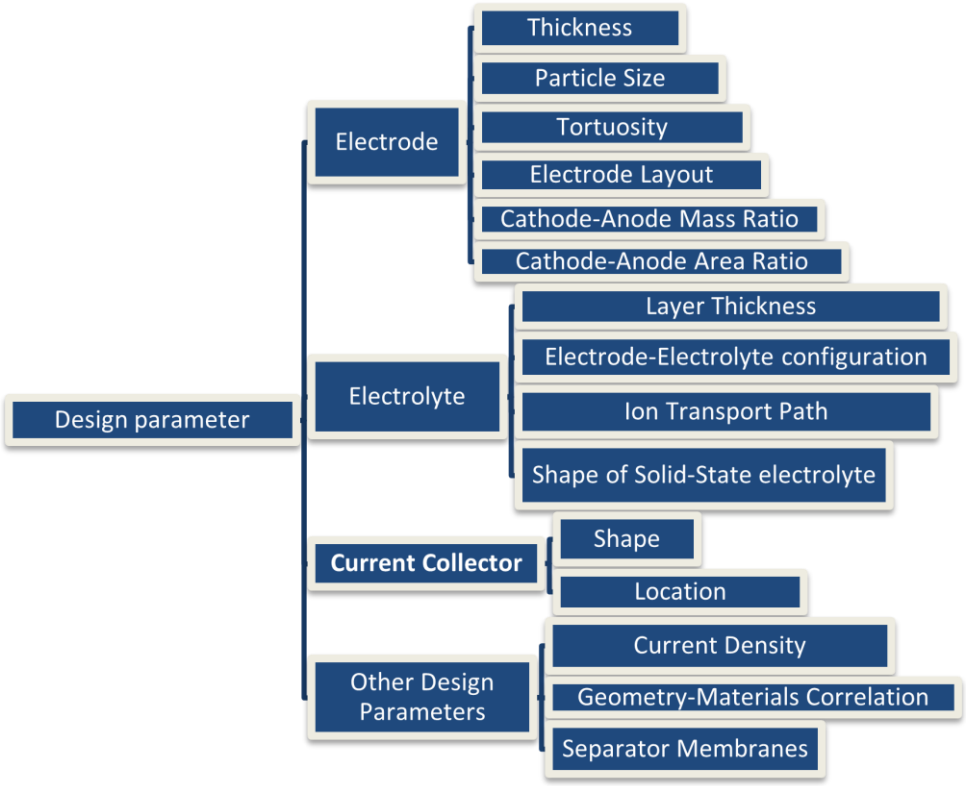


Figure 2.4 Design parameters for battery component

## 2.7 Structure of 18650 Li-ion Battery:

A cylindrical 18650 lithium-ion battery with a diameter of 18mm and a length of 65mm is frequently used because to its high energy density, extended cycle life, and dependability. In 1994, Panasonic created 18650 batteries to meet the rising need for smaller, lighter, longer-lasting storage batteries. The performance and safety of the battery are jointly determined by its structure, which is comprised of numerous essential components, including electrodes, a separator, an electrolyte, and design characteristics. *Figure 2. 5* Shows the internal structure of an 18650 Li-ion Battery. Many different types of cathode materials are used in 18650 batteries. Some of these materials include lithium cobalt oxide ($LiCoO_2$), which has a high energy density; lithium manganese oxide ($LiMn_2O_4$), which has thermal stability and safety; lithium nickel manganese cobalt oxide (NMC), which has a balance of properties; and lithium iron phosphate ($LiFePO_4$), which has excellent thermal stability and long cycle life. Graphite, silicon-graphite composites, and lithium titanium oxide (LTO) are the most common anode materials. Graphite has a high specific capacity and cycle stability but can be lithium plating at high charging rates. LTO is known for its excellent safety, fast charging, and long cycle life but has a lower energy density. The separator is usually constructed from polyethylene (PE) or polypropylene (PP), with ceramic-coated separators giving greater thermal stability and safety. The separator is an essential component that electrically separates the anode and cathode while enabling ionic conduction to conduct. Electrolytes are solutions of organic solvents like ethylene carbonate (EC), dimethyl carbonate (DMC), or diethyl carbonate (DEC) that contain lithium salts like lithium hexafluorophosphate (LiPF6). These solutions are balanced for viscosity, ionic conductivity, and stability, and they often contain additives that improve performance and safety. Battery Specifications are shown in *Table 1*.

Table 1: 18650 Battery Specifications[48]

| **Shape** | **Cylindrical lithium-ion battery** |
|---|---|
| Length | 65mm |
| Diameter | 18mm |
| Voltage range | 2 to 3.6 V |
| Nominal Voltage (V) | 3.3 |
| Nominal capacity | 1.1 Ah |
| Max Discharge Current (A) | 30 |
| Acceptable Temperature (°C) | −30 to 60 |
| Nominal Mass (g) | 39.8 |

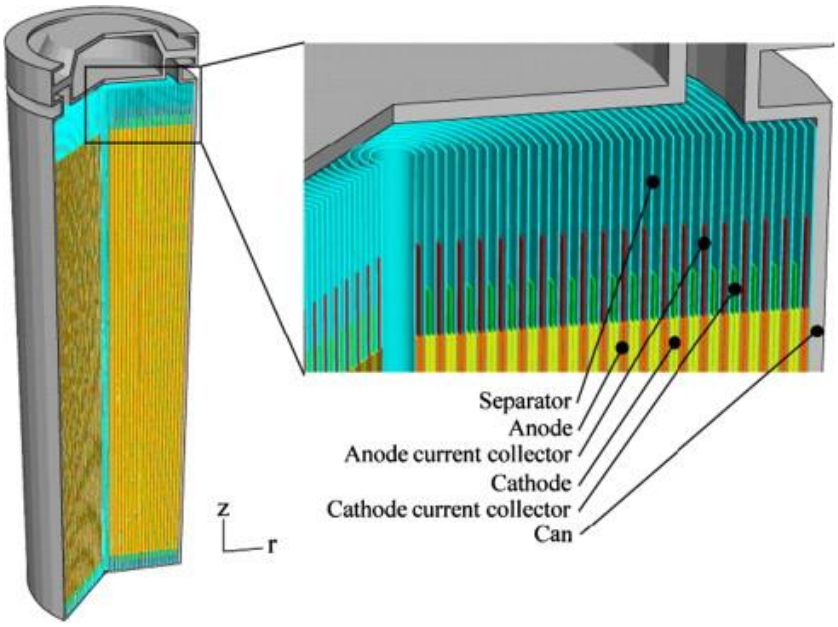


Figure 2. 5 internal structure of 18650 li ion battery [49]

## 2.8 The Pseudo-2-Dimensional (P2D) model:

The porous structure of Li-ion battery electrodes is crucial as it boosts the contact between solid materials and liquid electrolyte, speeding up slow chemical reactions. Yet, this complex setup makes it tough to create accurate battery models. In 1975, Newman and Tiedemann [18] tackled this issue by developing a theory for porous electrodes that simplified things by looking at average properties

instead of detailed shapes. Developing on this work, Doyle et al. [19] introduced the Pseudo-Two-Dimensional (P2D) model for Li-ion batteries in 1993. This model mixes the porous electrode theory with another theory for concentrated solutions, becoming one of the most popular models for Li-ion batteries. It views electrodes as a network of tiny particles surrounded by electrolytes, where lithium ions move in and out. The model uses a one-dimensional approach since movement is mostly in one direction. The P2D model has several key equations: one for lithium-ion movement inside solid particles, another for their movement through the electrolyte, and others for electrical potentials in both solid and liquid parts. It also includes an equation for reaction rates at particle surfaces. Experiments have proven the P2D model's accuracy, making it a go-to when real data isn't available. However, fully solving the P2D model equations is tricky, so various number-crunching methods like Finite-Difference, Finite-Element, and Finite-Volume are used to get close answers. These methods can be applied using special software like COMSOL and Battery Design Studio, which help simulate more complex battery designs.

## 2.9 Temperature effect on LIBs

Temperature effect on LIBs can divided into two parts such as low-temperature effect and high-temperature effect. Acceptable Temperature of 18650 LIBs ranged from -30°C to 60°C. The chemical reaction occurring in LIBs depends on which materials are used for this chemical analysis. Most of the time, this reaction is related to the temperature effect of the battery. Temperature variation can impact on the chemical reaction rate into the battery. Arrhenius equation shows a relation of rate of chemical reaction and reaction temperature. Moreover, not only are chemical reactions affected by the temperature, but also ionic conductivities of electrodes and electrolyte influences temperature.

At low temperatures below 25°C, the performance of lithium-ion battery will degrade. Nagasubramanian [39] did an experimental investigation using Panasonic 18650 LIBs at temperature range 25°C to -40°C and showed that power density and energy density was reduced 95% to 98.75% at low temperature (-40°C ) Performance degradation happens in several sources. firstly, it effects the property of electrolyte due to the viscosity of electrolyte increase at low temperature which will reduce ionic conductivity. Consequently, the internal resistance will increase due to the rise of the impedance. Bugg et al describe the formulation of electrolyte at low temperature which will apply for space applications. Another factor that impact on performance degradation of LIBs at low temperature is raising the charge-transfer resistance. At -20°C LFP based positive electrode gives three times higher charge transfer resistance compared to room temperature, this will affect kinetics of the battery largely. It is more difficult to charge a battery in low temperature then discharging it because the charge transfer resistance for charging is much lower than discharging. Besides, the diffusion of li ion in electrode is become too slow at low temperature with low activation energy that cause the degradation of battery. Low temperature can cause anode polarization, causing graphite and carbon-based anodes to approach lithium metal potential when charging, slowing lithium-ion intercalation. As a result, the surface of the electrodes accumulates lithium ions that are known as lithium plating, which reduces the battery capacities. Moreover, the lithium plating takes the form of dendritic, which can pass the separators and cause the internal short-circuit.

When LIBs are in operation such as charging or discharging, heat is produced due to the chemical reaction inside the battery. It is very critical to measure high temperature effects at LIBs. Paul et al. [40] also conducted an experiment analysis of 5.2 Ah capacity 18650 LIBs at temperature ranged from

28°C to 100°C and shows that huge capacity drops between 1st and 2nd cycle above 50°C temperature moreover after 70°C discharge capacity faded.

## 2.10 Heat Generation in Li ion Battery

Heat generated within LIBs at room temperature is often linked to chemical processes and charge transfer during charging and discharging[18-19]. In LIBs, heat is created by either a reversible or irreversible mechanism[33], [51], [52]. Figure 5 depicts the probable heat production within LIBs. The reversible process makes entropic heat, which comes from the change in entropy that can happen during electrochemical reactions[53]. Many irreversible processes can create heat, including active polarization, ohmic heating, mixing-induced heating, and enthalpy change [54], [55], [56]. Polarization happened because the batteries had an overpotential between their working potential and their open circuit potential. Different process of heat generation is shown in *Figure 2.6*. It causes an increase in charge transfer resistance at the electrode-electrolyte interface, or Solid Electrolyte Interface (SEI). Heat is generated at the contact when lithium ions overcome this resistance to intercalate or deintercalated. Ohmic heating takes place in the electrolyte as well as the electrode. The resistance of electrodes and electrolytes impedes charge transmission[7]. The homogeneity of the ion distribution during LIB operation (charging or discharging) provides rise to the possibility of ion mixing and the subsequent generation of heat. Another type of heat-generation irreversible process is the enthalpy change associated with phase transitions in cathodes, which mostly occur because of lithium-ion diffusion[57].

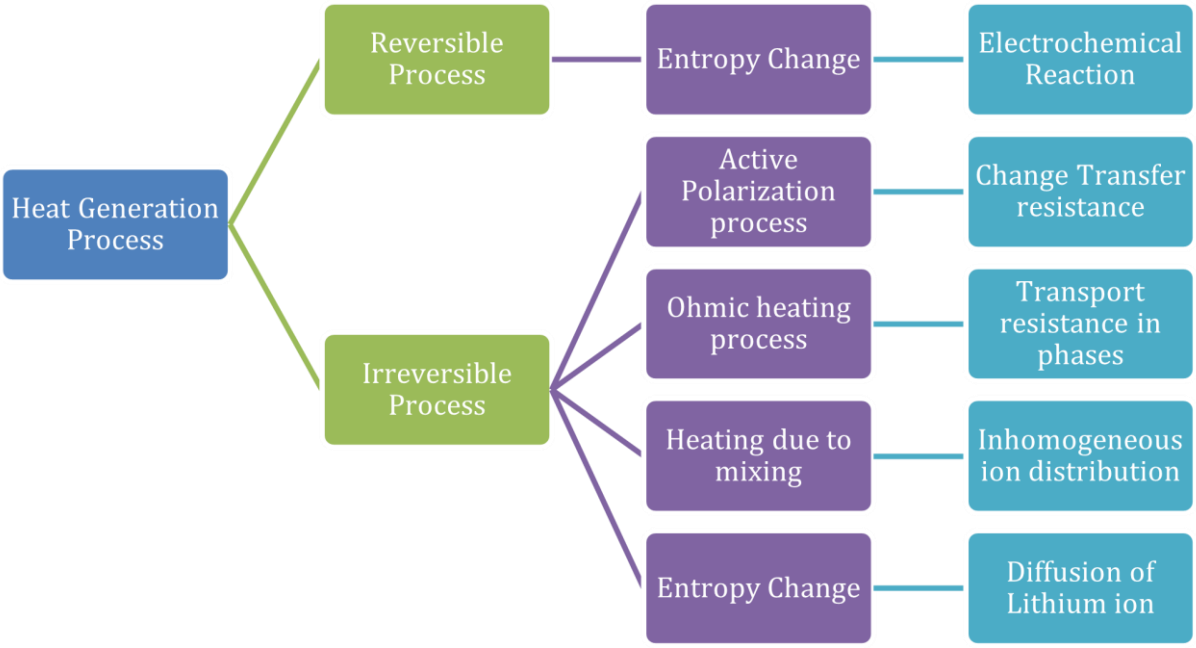


Figure 2.6 Representation of the various kinds and processes of heat production in LIBs

# Chapter 3

## 3.1 Research Methodology

This chapter presents a comprehensive analysis of the research procedure carried out. This study evaluates the electrochemical and thermal performance of commercial 18650M1A cells designed with various electrode configurations. A comprehensive approach was chosen to investigate the effect of different design choices on cell behaviour. Figure 3.1 displays a flow diagram showing the research method, presenting a clear and systematic summary of the methods followed in this work.

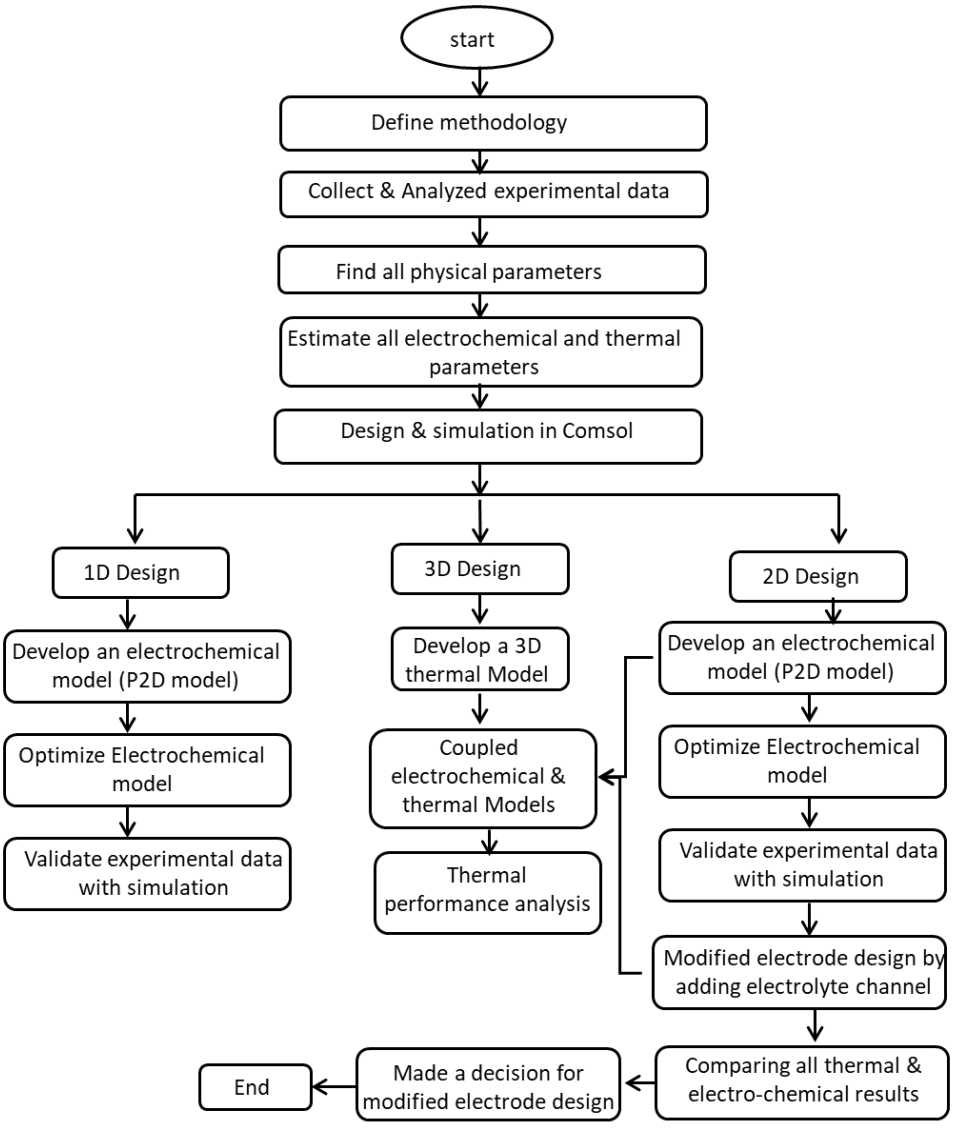


Figure 3.1 Flow diagram of the research procedure

## 3.2 Experimental data analysis

To determine the performance of commercial 18650 lithium iron phosphate (LFP) batteries made by A123 Systems (Part #APR18650M1A, 1.1 Ah), Sandia National Laboratories (SNL) carried out a comprehensive charging and discharging test. to evaluate how well they function, how long they last, and how safe they are in various operating environments. The test consisted of a series of charge-discharge cycles, in which the cells were charged using a constant current (CC) phase, followed by a constant voltage (CV) phase, and then discharged at various rates (C-rates) until they reached a safe cutoff voltage. The test was carried out at a variety of temperatures. An accurate study of voltage, current, temperature, and capacity was possible using temperature-controlled chambers that simulated real-world circumstances and continuous data logging. This charging-discharging voltage and temperature data is stored as open source on the battery archive website[58]. In the current study, we collect this open-source data as experimental data and then analyse this dataset to determine the voltage value and the cell's temperature at 298.15K.

## 3.3 Simulation Procedure

This study comprehensively evaluated the electrochemical and thermal performance of an 18650 cylindrical lithium-ion battery. Numerical analysis was done by using COMSOL Multiphysics battery design module version 6.2. The research involved coupling a 1D electrochemical model with a 3D thermal model. While the model's 1D and 2D designs employed the same underlying equations and methodologies, the 2D design analysis was explicitly utilized to assess the effects of electrode design modifications, such as the addition of electrolyte channels and battery performance. The cells studied consisted of a graphite anode, a lithium iron phosphate ($LiFePO_4$) cathode, and a liquid electrolyte comprising 1.2 M $LiPF_6$ in ethylene carbonate/ethyl methyl carbonate (EC/EMC = 3/7, v/v). Initially, the 1D model is developed to parameterize all electrochemical parameters such as kinetics (reaction rate constant), diffusion coefficient, etc. Using the optimization module, validate the 1D electrochemical model with experimental data. This simulation procedure was followed by the COMSOL Multiphysics application libraries[59].

Moreover, the 2D simulation using a P2D electrochemical framework solved governing equations for lithium-ion diffusion using Fick's law [60], ionic and electronic conduction through Ohm's law, and reaction kinetics via the Butler-Volmer equation[61]. This model described vital processes such as the insertion and extraction of lithium ions between graphene layers and ion transport within the electrolyte. Heat generation within the battery was subdivided into three main contributions[33]: ohmic heat, arising from ionic and electronic resistances; reaction heat, due to entropy changes in the electrochemical reactions; and polarization heat, resulting from overpotentials at the electrode/electrolyte interface. These contributions were calculated and transported to a 3D thermal model to evaluate the spatial temperature distribution.

Fourier's law of heat conduction[62] served as the foundation for the three-dimensional thermal model, which considered convective and radiative heat losses from the battery's surfaces and thermal transport through the battery. The thermal study relied significantly on the density, specific heat, and thermal conductivity of the battery components, electrodes, separator, and case. This coupling enabled bidirectional feedback, in which the thermal model influenced temperature-dependent electrochemical behaviours, and the electrochemical model updated the heat source distribution.

However, the 2D model made it possible to examine in greater depth how changes to the electrode structure, like adding electrolyte channels, affect heat behavior and ionic conductivity. These improvements aimed to improve ion transport, decrease overpotentials, and reduce localized hotspots. The heat generation profile from the two-dimensional domain was transferred to the three-dimensional thermal model, facilitating a coupled simulation that assessed both localized and bulk thermal effects.

Meshing is a critical element of simulations for achieving accuracy and convergence. A user-defined finest mesh was employed in the 1D model to discretize high-resolution electrochemical domains, ensuring an accurate representation of gradients in lithium concentration and potential across the electrode and electrolyte layers. The two-dimensional model employed a structured triangular mesh to incorporate design modifications like electrolyte channels. This configuration enabled the uniform distribution of elements within the active material, effectively capturing steep gradients near the electrolyte channels and boundaries. Boundary layer meshing was employed along the channel walls to resolve ionic flux and potential gradients accurately. The meshing strategy was refined to balance computational efficiency and result precision.

A high-quality tetrahedral mesh was employed to model the battery's complex geometry in the 3D thermal domain, encompassing the active material, mandrel, connectors, and air-cooling compartment. The refined tetrahedral mesh effectively captured heat conduction and convection effects from the surrounding airflow. The meshing was notably refined in areas with anticipated steep temperature gradients, including near the cooling boundaries and interfaces between distinct materials. This meshing approach ensured accuracy in thermal distribution and feedback to the electrochemical models while maintaining computational feasibility.

The findings indicated that the electrochemical-thermal coupled model effectively predicts bulk battery behaviour and average thermal performance. The coupled model provided enhanced spatial resolution, facilitating a thorough evaluation of localized thermal gradients and the effects of structural modifications. Embracing electrolyte channels enhanced thermal uniformity, decreased peak temperatures, and improved overall performance by optimizing ion transport pathways.

This comprehensive framework combines 1D, 2D, and 3D design analyses and highlights the significance of material composition, structural design, and sophisticated meshing techniques to optimize lithium-ion batteries. By simulating and comparing simple and comprehensive models, $LiFePO_4$-based 18650 lithium-ion batteries may be more operationally efficient and thermally balanced.

# Chapter 4

## Model development

### 4.1 Cell Design

#### 4.1.1 1D Cell Design

The 1D cell design simplifies the structure of a lithium-ion battery by focusing on its layers along the thickness direction. This approach makes it easier to study the battery's electrochemical behaviour. At the starting point of the model is the negative current collector ($L_{n,cc}$), which is $1.0 \times 10^{-5}$ m thick. It collects electrons from the negative electrode ($L_n$), a layer $1.6 \times 10^{-5}$ m thick that stores lithium ions during discharge. Next comes the separator ($L_s$), $1.8 \times 10^{-5}$ m thick, which allows ions to flow between the electrodes while preventing them from touching. Following this is the positive electrode. ($L_p$), which is $8.1 \times 10^{-5}$ m thick and releases lithium ions during discharge. At the end of the model is the positive current collector ($L_{p,cc}$), $1.9 \times 10^{-5}$ m thick, which carries electrons from the positive electrode to the external circuit. 1D cell design of 18650 Li-ion battery shown in Figure 4.1.

The current collectors are made of copper on the negative side and aluminium on the positive side. The active materials are graphite on the anode and lithium iron phosphate (LFP) on the cathode. In the 1D model, the current collectors are represented at the starting and ending points of the structure. This simplified design provides a clear and efficient way to study the battery's performance.

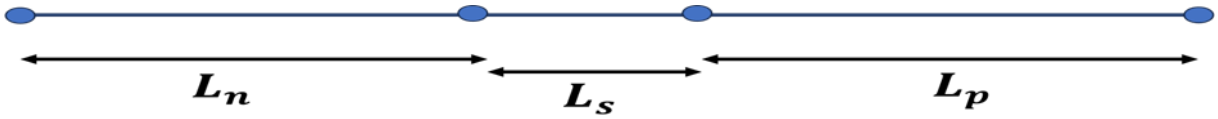


Figure 4.1 1D Cell Design

#### 4.1.2 2D Cell Design

In this study, four major types of 2D cell designs have been developed to assess the effects of structural changes on lithium-ion battery performance, as depicted in Fig. The first design, (a), is the conventional cell design with a negative electrode of graphite, a separator, and a positive electrode of LFP. This design is like a 1D structure and is used as a reference design for comparison. The changes made to the designs include incorporating pathways for the transport of electrolytes and ions within the electrodes. In design (b), only the negative electrode (graphite) contains the channels, whereas the positive electrode is uniform. On the other hand, design (c) has only channels in the positive electrode (LFP) without any changes in the negative electrode. Last of all, design (d) incorporates channels into both the negative and positive electrodes so that there are more paths for ions to travel across the entire cell. 2D cell design of 18650 Li-ion battery shown in *Figure 4.2*.

The 2D design of our electrolyte channel is based on catheter-like structures in the xylem of tree trunks that allow nutrients to be transported from the roots to the crown. As these xylem structures facilitate nutrient transport in plants, introducing electrolyte channels into the electrodes will significantly

improve lithium-ion transfer. This bio-inspired approach solves the problems of thick electrodes, especially during discharging, by providing more channels for ion transport.

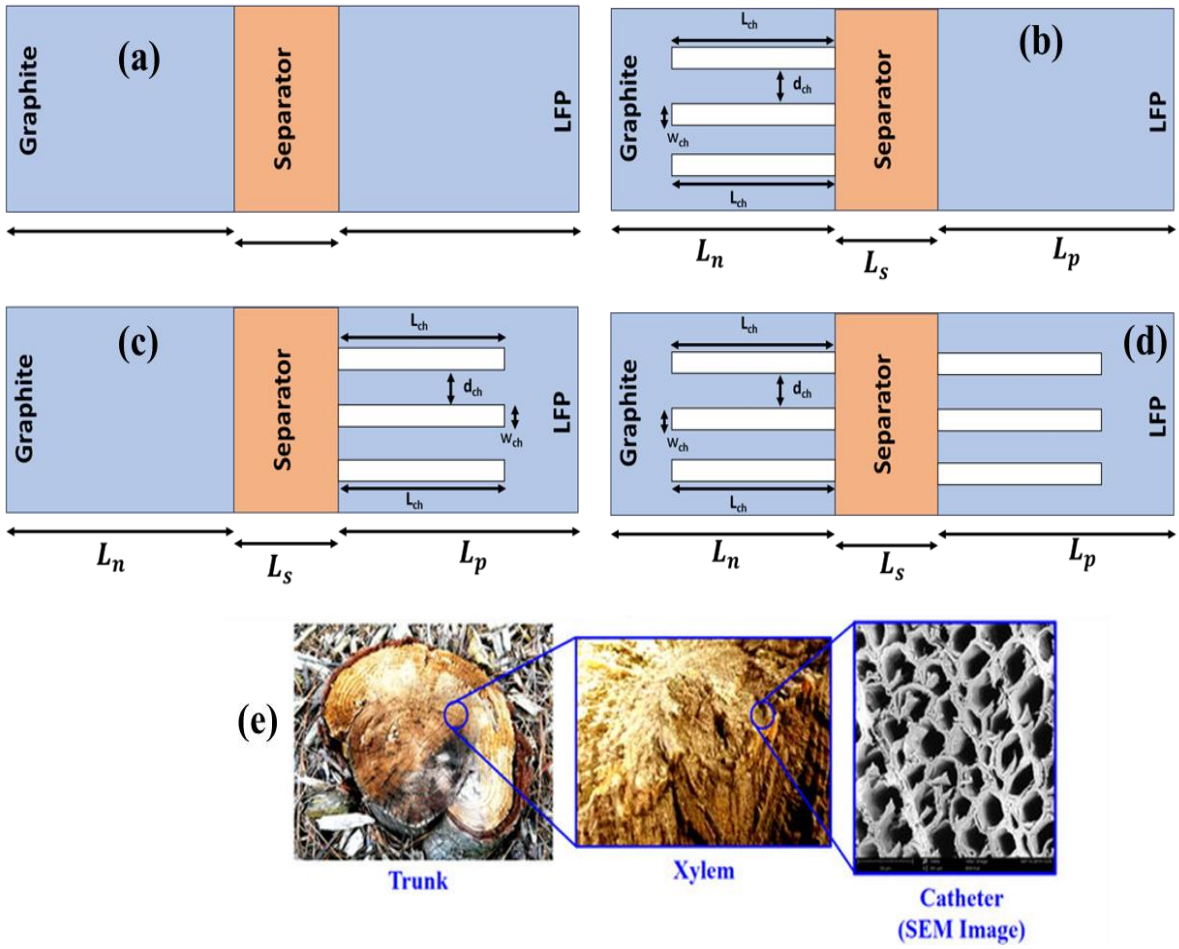


Figure 4.2 2D Cell Design: (a) Standard cell (b) Channel in negative electrode (c) Channel in positive electrode (d)Channel in both electrodes (e) The electrolyte channel's design was influenced by the structure of a catheter, which assists in the transportation of nutrients through the xylem of a trunk [35].

These factors define the impact of these channels on cell performance, and therefore, their design parameters are essential. The channel thickness, $(L_{ch})$ Is adjusted to investigate the effect of the depth of the channels on ion transport. In the same way, the channel width $(w_{ch})$, which varies over a particular range to investigate its effect on the distribution of electrolytes and ionic conductivity. The distance between two consecutive channels $(d_{ch})$, is also considered because this parameter determines the packing density of the channels inside the electrode material and the ease of access of the ions to the channels. Furthermore, the number of channels in each design differs to investigate channel density's effects on electrochemical performance.

The height of the cell is represented by $(h_{batt})$, which is much greater than cell thickness. To simplify the analysis and avoid numerical problems arising from the difference in scale between the variables,

the height is scaled by dividing h by 1000, and the scaled height is represented by $h'_{batt}$. This normalization helps scale all designs and makes it easier to represent geometrical parameters in simulations and computations.

A parametric analysis is carried out by systematically changing these parameters to determine the optimum design parameter. For instance, the channel width is defined between 0 to 100nm, the thickness of the channel varies between 0 to 10 µm, and the number of channels is tuned between 0 and 8. This extensive assessment allows for identifying how channel geometry and position affect the distribution of electrolytes, the transport of ions, and the overall cell performance, ultimately determining the best design.

### 4.1.3 3D Cell Design

The design of a cylindrical 18650 lithium-ion battery incorporates a structured and optimized configuration to balance electrochemical performance, thermal management, and structural integrity. At the battery's core is the mandrel, with a radius of 2 mm, constructed from nylon as an insulating material. The mandrel serves as the central axis, supporting the tightly wound layers of the battery's internal components. 3D design of 18650 Li-ion battery with flow compartment exhibits in *Figure 4.3*.

Mandrel is the surrounded by active battery material, consisting of cathode, anode, and separator layers. These materials are arranged in a cylindrical configuration with a height of 65 mm and an outer radius of approximately 9 mm, forming the core region where energy storage and electrochemical reactions occur. Encasing the active material is the outer shell, known as the can. This shell, typically made of steel, ensures mechanical stability and protects the internal components from external damage and environmental influences. The design also integrates a battery connector at the top of the can. This connector, with a thickness of 3 mm, facilitates electrical connections and ensures compatibility with external circuits. To manage thermal behaviour, the battery operates within a flow compartment where air flows over the surface of the battery. Using laminar airflow, air enters through an inlet, flows along the surface, and exits through an outlet, effectively dissipating heat generated during operation.

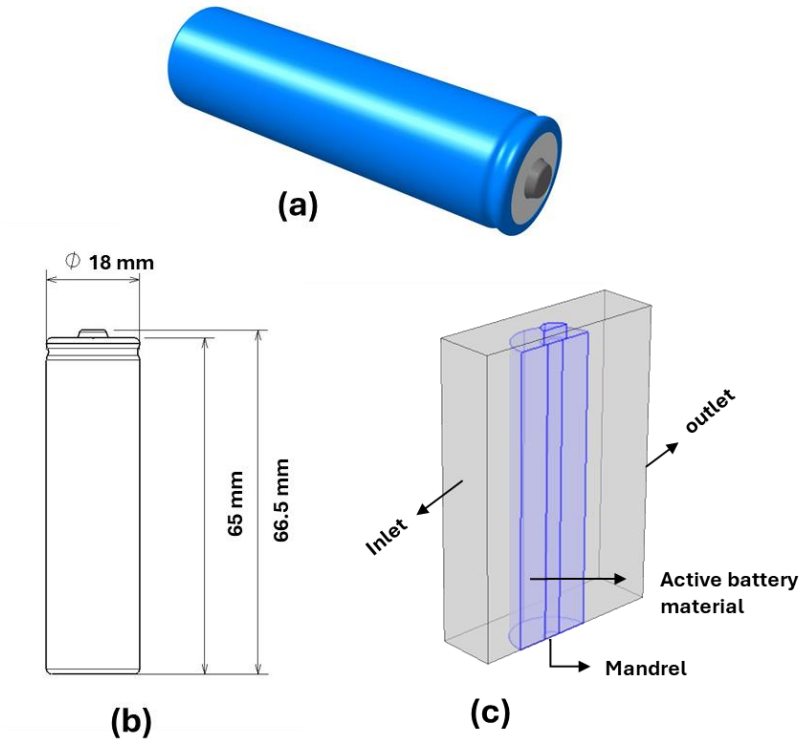


Figure 4.3 Model of 18650 Battery (a) Isometric view (b) Front view with dimension (c) Flow Compartment

## 4.2 Cell Information

The physical, geometrical, thermodynamic, kinetic, thermal, and transport parameters used in the electrochemical and thermal model of cylindrical lithium-ion battery cells are presented in *Table 2*. These parameters are essential in the simulation of cell behaviour under various operating conditions. The model employs simulations in several dimensions to enhance the electrolyte channel performance analysis. One-dimensional (1D) simulations confirm the model by concentrating on the electrochemical processes. Two-dimensional (2D) analysis gives information on the geometry for various designs. Thermal analysis of the cell is done using three-dimensional (3D) geometry to determine heat generation and removal in the cell. The cells investigated included a graphite anode, a lithium iron phosphate ($LiFePO_4$) cathode, and a liquid electrolyte of 1.2 M LiPF6 in a mixture of ethylene carbonate and ethyl methyl carbonate (EC/EMC = 3/7).

The simulations also demonstrate how the cell performs during discharge at various C-rates, for example, 1C, 2C, and 3C, and how operating conditions influence the cell's performance. Table I gives a clear description of the parameters used in the model. It also contains descriptions, typical values, units, and their simulation use. These parameters are obtained from the literature [32] [48][63] and the in-built COMSOL database so that the data set is credible. This information assists in the correct positioning of the model and guarantees the exactness of the predictions.

Table 2: List of Model Parameters [32][48][63]

| Parameter | Description | Value |
|---|---|---|
| $L_p$ | Positive electrode thickness | $8.1\times10^{-5}$ m |
| $L_n$ | Negative electrode thickness | $3.6\times10^{-5}$ m |
| $L_s$ | Separator thickness | $1.8\times10^{-5}$ m |
| $L_{p,cc}$ | Positive current collector thickness | $1.9\times10^{-5}$ m |
| $L_{n,cc}$ | Negative current collector thickness | $1\times10^{-5}$ m |
| $\mathrm{L}_{cell}$ | Cell thickness | $1.6\times10^{-4}$ m |
| $\varepsilon_{l,n}$ | Electrolyte phase volume fraction of negative electrode | 0.25 |
| $\varepsilon_{l,p}$ | Electrolyte phase volume fraction of positive electrode | 0.26 |
| $\varepsilon_{l,s}$ | Electrolyte phase volume fraction of separator | 0.37 |
| $\varepsilon_{s,n}$ | Solid phase volume fraction of negative electrode | 0.733 |
| $\varepsilon_{s,p}$ | Solid phase volume fraction of positive electrode | 0.74 |
| $\mathrm{r_n}$ | Particle radius negative electrode | $3\times10^{-6}$ m |
| $\mathrm{r_p}$ | Particle radius positive electrode | $5\times10^{-7}$m |
| $\mathrm{h_{batt}}$ | Battery height | 0.065 m |
| $h_{batt}^{'}$ | Normalize battery height | $0.065\times10^{-3}$ m |
| $\mathrm{r_{batt}}$ | Battery radius | 0.009 m |
| $\mathrm{r_{man}}$ | Mandrel radius | 0.002 m |
| $k_p^0$ | reaction rate constant of positive electrode | $2\times10^{-10}$ $ms^{-1}$ |
| $k_n^0$ | reaction rate constant of negative electrode | $2\times10^{-10}$ $ms^{-1}$ |
| $C_{s,n}^0$ | Initial concentration of lithium in solid phase negative electrode | 30232 $molm^{-3}$ |
| $C_{s,p}^0$ | Initial concentration of lithium in solid phase Positive electrode | 2297.7 $molm^{-3}$ |
| $C_l^0$ | Initial electrolyte salt concentration | 1200 $molm^{-3}$ |

| | | |
|---|---|---|
| $C_{s,n}^{max}$ | Maximum lithium concentration in the solid phase of negative electrode | 30537molm$^{-3}$ |
| $C_{s,p}^{max}$ | Maximum lithium concentration in the solid phase of Positive electrode | 22836 molm$^{-3}$ |
| $\sigma_p$ | Solid phase conductivity of Positive electrode | 91 Sm$^{-1}$ |
| $\sigma_n$ | Solid phase conductivity of negative electrode | 100 Sm$^{-1}$ |
| $D_{s,p}^{0}$ | Initial diffusion coefficient in the solid phase of Positive electrode | 8.6×10$^{-19}$×a m$^2$s$^{-1}$ |
| $D_{s,n}^{0}$ | Initial diffusion coefficient in the solid phase of negative electrode | 1×10$^{-11}$ m$^2$s$^{-1}$ |
| $E_{k,p}$ | Activation energy of kinetics of Positive electrode | 30000 J mol$^{-1}$ |
| $E_{k,n}$ | Activation energy of kinetics of negative electrode | 20000 J mol$^{-1}$ |
| $E_{d,p}$ | Activation Energy of Diffusion of Positive electrode | 17500 J mol$^{-1}$ |
| $E_{d,n}$ | Activation Energy of diffusion of negative electrode | 35000 |
| $T_{Inlet}$ | Inlet Temperature | 298.18 K |
| F | Faraday constant | 96485 C mol$^{-1}$ |
| R | Ideal gas constant | 8.314 Jmol$^{-1}$k$^{-1}$ |

## 4.3 Modelling of Lithium-ion Battery

### 4.3.1. Electrochemical Modelling

Doyel [64] has developed the P2D electrochemical model applied in this work. It describes a battery as having five layers stacked together: the anode current collector, the anode, the separator, the cathode, and the cathode current collector, as illustrated in *Figure 4.4*. The electrodes are comprised of a series of spherical elements distributed uniformly, the gaps between them being filled with a separator and an electrolyte. Electrode particles do not react with themselves or the electrolyte in regions where the two do not come into contact. In charging or discharging, the lithium ions are formed and travel in one way in the electrolyte and the electrodes, though the free electrons remain within the particles. When one electrode dissolves into the electrolyte, lithium ions, an equivalent number of free electrons in the electrode is produced to balance the charge. The ions continue to the opposite electrode of the separator while the electrons move through an electric circuit. Both are also met again at the other electrode interface between particles and electrolyte.

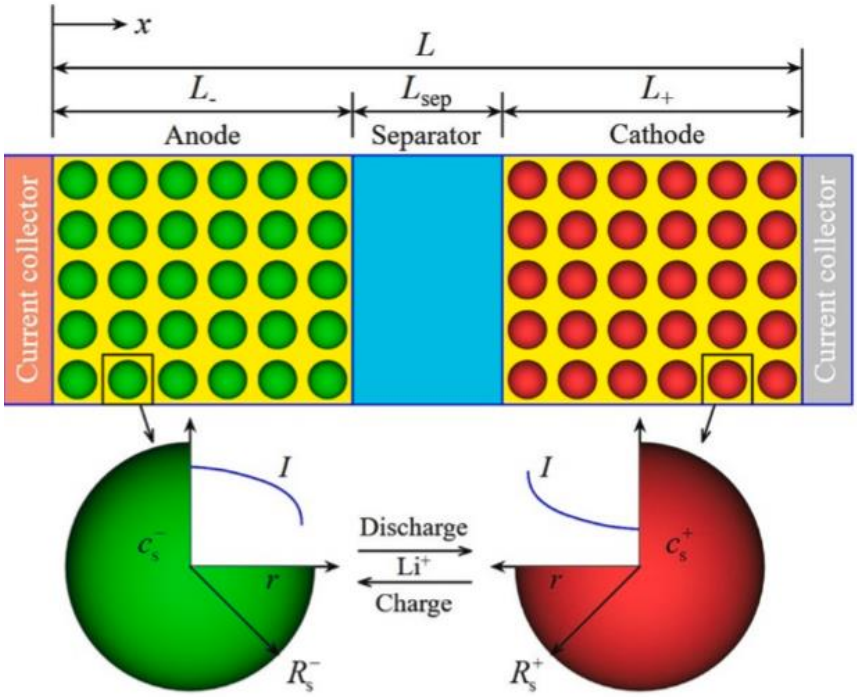


Figure 4.4 Schematic of a P2D lithium-ion battery model [65]

The governing equations for the electrochemical system are derived from mass conservation, charge conservation, and electrochemical kinetics. They provide a detailed mathematical description of the processes in the anode, separator, and cathode regions.

**Mass Conversion Equations:**

**Solid Phase (Lithium Diffusion)**

In the solid phase, lithium ions diffuse radially within active material particles. Fick's second law describes this diffusion [60]:

$$\frac{\partial c_s}{\partial t} = \begin{cases} D_{s,n}\frac{1}{r^2}\frac{\partial}{\partial r}\left(r^2\frac{\partial c_{s,n}}{\partial r}\right), & \text{Anode } (0 < x < L_n) \\ D_{s,p}\frac{1}{r^2}\frac{\partial}{\partial r}\left(r^2\frac{\partial c_{s,p}}{\partial r}\right), & \text{Cathode } \left(L_n + L_s < x < L_n + L_s + L_p\right) \end{cases} \quad (14)$$

In eq. (14), $C_s$ is the lithium concentration in the solid phase, $D_s$ is the diffusion coefficient, and r is the radial coordinate within the particle. These equations describe the radial diffusion of lithium within the solid phase. At the surface of the particles, the lithium flux is directly proportional to the reaction current density (j), linking the transport within particles to the interfacial reaction kinetics. The boundary conditions ensure symmetry at the particle centre and a flux proportional to the reaction current density (j) at the particle surface.

At the particle centre (r=0):

$$\frac{\partial c_s}{\partial r} = 0 \tag{15}$$

At the particle surface ($r=R_p$):

$$-D_{s,n}\frac{\partial c_{s,n}}{\partial r} = j_n, \; -D_{s,p}\frac{\partial c_{s,p}}{\partial r} = j_p \tag{16}$$

**Liquid Phase (Electrolyte Diffusion)**

In the electrolyte, lithium-ion concentration evolves due to diffusion and migration under concentration gradients and reaction fluxes at the electrode-electrolyte interfaces:

$$\epsilon_l \frac{\partial c_l}{\partial t} = \begin{cases} \frac{\partial}{\partial x}\left(D_{l,n}^{\text{eff}}\frac{\partial c_{n,n}}{\partial x}\right) + a_s(1-t^+)j_n, & \text{Anode } (0 < x < L_n) \\ \frac{\partial}{\partial x}\left(D_{l,s}^{\text{eff}}\frac{\partial c_{,s}}{\partial x}\right), & \text{Separator } (L_n < x < L_n + L_s) \\ \frac{\partial}{\partial x}\left(D_{l,p}^{\text{eff}}\frac{\partial c_{l,p}}{\partial x}\right) - a_s(1-t^+)j_p, & \text{Cathode } \left(L_n + L_s < x < L_n + L_s + L_p\right) \end{cases} \tag{17}$$

In eq. (17), $C_l$ is the concentration of lithium ions in the electrolyte, $\epsilon_l$ is the volume fraction, and $t^+$ is the transference number. Continuity at the interfaces ensures seamless lithium-ion transport across different regions of the cell. In the separator, where no reactions occur, diffusion is the only mode of transport.

At the ends of the cell ($x=0, x=L_n+L_s+L_p$):

$$\frac{\partial c_l}{\partial x} = 0 \tag{18}$$

Eq. (18) reflects the diffusion of lithium ions in the electrolyte and their consumption or generation at the electrode-electrolyte interface. The effective diffusivity ($D_{\text{eff},l}$) accounts for the porosity and tortuosity of the porous electrodes and separator.

**Charge Conservation Equations**

The charge conservation equations describe the transport of electrons in the solid phase and lithium ions in the electrolyte phase, maintaining the electrochemical potential balance.

**Solid Phase (Electron Conduction)**

The electron current in the solid phase follows Ohm's law:

$$\sigma_{\text{eff}}\frac{\partial^2 \phi_s}{\partial x^2} = \begin{cases} a_s j_n, & \text{Anode } (0 < x < L_n) \\ a_s j_p, & \text{Cathode } \left(L_n + L_s < x < L_n + L_s + L_p\right) \end{cases} \tag{19}$$

In eq. (19), $\phi_s$ is the solid-phase potential, $\sigma_{eff}$ is the effective conductivity of the solid, and j is the reaction current density. Boundary conditions define the potential at the anode and cathode current collectors.

At the current collectors:

$$\phi_s = \phi_s^0 \tag{20}$$

Eq. (20) ensures the conservation of charge in the solid phase, with the reaction current density (j) acting as a source term.

**Liquid Phase (Ionic Conduction)**

The ionic conduction in the electrolyte is governed by a modified Ohm's law that includes both migration and diffusion contributions:

$$-\frac{\partial}{\partial x}\left(\kappa_{\text{eff}}\frac{\partial \phi_l}{\partial x}\right)+\frac{2\kappa_{\text{eff}}RT(1-t^+)}{F}\frac{\partial c_l}{\partial x}=\begin{cases}a_s j_n, & \text{Anode } (0<x<L_n)\\ 0, & \text{Separator } (L_n<x<L_n+L_s)\\ a_s j_p, & \text{Cathode } \left(L_n+L_s<x<L_n+L_s+L_p\right)\end{cases} \tag{21}$$

In eq. (21), $\phi_l$ is the electrolyte potential, $\kappa_{eff}$ is the effective ionic conductivity, and RT/F represents thermodynamic factors. Continuity across interfaces ensures a consistent potential profile.

At the ends of the cell (x=0, $x=L_n+L_s+L_p$):

$$\frac{\partial \phi_l}{\partial x}=0 \tag{22}$$

Eq. (22) captures the ionic conduction and concentration polarization effects in the electrolyte.

**Butler-Volmer Equation**

The Butler-Volmer equation couples the electrode kinetics with the overpotential (η), driving the electrochemical reactions[61]:

$$j=Fk\left(c_s^{\max}-c_s^{\text{surf}}\right)^{0.5}\left(c_s^{\text{surf}}\right)^{0.5}\left(\frac{c_l}{c_{\text{ref}}}\right)^{0.5}\left[\exp\left(\frac{0.5F\eta}{RT}\right)-\exp\left(-\frac{0.5F\eta}{RT}\right)\right] \tag{23}$$

The overpotential (η) is calculated as:

$$\eta=\phi_s-\phi_l-E_{eq} \tag{24}$$

Eq. (23) integrates thermodynamic effect's reaction rate constants (k), and lithium concentration dependencies. It determines the reaction current densities at the anode ($j_n$) and cathode ($j_p$).

### 4.3.2 Thermal Modelling

In this model, the solid's ability to resist heat conduction is much less than the ability of the battery surface to resist heat convection. Therefore, the temperature of the cell's interior is thought to remain constant. More importantly, small changes in the temperature do not significantly alter the levels of chemistry within the cell. To address this, the electrochemical model is coupled with a thermal model where the over-temperature of the entire cell is determined. As a further assumption, it is considered that temperature fluctuations do not influence the activities of cell chemistry. The thermal behaviour of the cylindrical Li-ion battery is governed by the heat transfer equation, which describes the conduction of heat within the battery material and the interaction with its surroundings. The equation is expressed as:

$$\nabla \cdot (k\nabla T) + Q = \rho c_p \frac{\partial T}{\partial t} \tag{25}$$

In Eq. 25, T is the temperature(K), k is the thermal conductivity (W $m^{-1}$ $K^{-1}$),Q represents the volumetric heat source (W/$m^3$), $\rho$ is the density (kg $m^{-3}$), $C_P$ is the specific heat capacity (J $kg^{-1}$ $K^{-1}$) and time (t) is in sec. The first term, k∇T captures heat conduction within the battery, while the second term, Q, accounts for internal heat generation. The term $\rho c_p \frac{\partial T}{\partial t}$ represents transient heat storage, accounting for the dynamic temperature response of the battery material.

The thermal conductivity in the active material is anisotropic due to the spiral-wound structure of the battery layers. Thermal conduction is characterized by radial $k_T$, angular $k_\theta$, and axial components $k_z$, which vary significantly depending on the material's geometry. To represent this anisotropy, the thermal conductivity tensor is used, transformed appropriately for the cylindrical coordinate system. Heat conduction follows Fourier's law[62], where the heat flux is proportional to the negative temperature gradient, expressed as

$$q = -\mathrm{k}\nabla\mathrm{T} \tag{26}$$

In eq.26, q is the heat flux vector (W/$m^2$). Heat generation in the battery arises from multiple sources. There are three parts of heat sources during charge and discharge processes, including reaction heat $Q_{rea}$, ohmic heat $Q_{ohm}$ and active polarization heat $Q_{act}$. The energy conversation equation in the lithium-ion battery is given by[33]

$$L_i \rho_i C_{p,i} \frac{\partial T}{\partial t} + \nabla \cdot \left(\frac{-k_i}{L_i} \nabla T\right) = L_i (Q_{\mathrm{rea}} + Q_{\mathrm{act}} + Q_{\mathrm{ohm}}) \tag{27}$$

active polarization heat generation rate is [33]

$$Q_{\mathrm{act}} = S_{a,j} j_{\mathrm{loc},i} \left(\phi_{1,i} - \phi_{2,i} - U_i\right) \tag{28}$$

The total reaction heat generation rate is[33]

$$Q_{\text{rea}} = S_{a,i} j_{\text{loc},i} T \frac{\partial U_i}{\partial T} \tag{29}$$

Ohmic heat generation rate is[33]

$$Q_{\text{ohm}} = \frac{\sigma^{\text{eff}}}{L_i^2} \nabla\phi_1 \cdot \nabla\phi_1 + \frac{\kappa^{\text{eff}}}{L_i^2} \nabla\phi_2 \cdot \nabla\phi_2 + \frac{\kappa_D^{\text{eff}}}{L_i^2} \frac{\nabla c_2}{c_2} \cdot \nabla\phi_2 \tag{30}$$

Active heat $Q_{\text{act}}$ and ohmic $Q_{\text{ohm}}$ are irreversible, while reaction heat $Q_{\text{rea}}$ is reversible.

$$\begin{aligned} Q_{\text{irr}} &= Q_{\text{act}} + Q_{\text{ohm}} \\ Q_{\text{re}} &= Q_{\text{rea}} \end{aligned} \tag{31}$$

Boundary conditions are applied to simulate the thermal environment of the battery accurately. At the inlet boundary, the temperature is fixed, representing a controlled cooling system, while an outflow condition ensures zero heat flux at the outlet. Symmetry boundaries are assumed to be thermally insulated. The initial temperature of the battery is uniform at 298.15K, representing ambient conditions.

The model incorporates the Navier-Stokes equations [66] to simulate airflow around the battery, enabling the analysis of convective cooling. The governing equations for incompressible laminar flow are:

Momentum Conservation:

$$\rho\left(\frac{\partial u}{\partial t} + (u \cdot \nabla)u\right) = -\nabla p + \mu\nabla^2 u \tag{32}$$

Continuity Equation:

$$\nabla . u = 0 \tag{33}$$

In eq. 32, u is the air velocity (m/s), P is the pressure (Pa), μ is the dynamic viscosity (Pa.s) and ρ is the fluid density (kg/m$^3$).Boundary conditions for the airflow include a specified velocity at the inlet and a fixed pressure condition at the outlet; no-slip conditions are applied at the battery walls, ensuring that the fluid velocity relative to the surface is zero. These equations allow the simulation of laminar airflow patterns and the resulting convective heat transfer. The continuity equation ensures mass conservation in the incompressible fluid.

*Table 3:* Thermal property parameters for each material of the battery.

| Materials | $k_T$ (W m$^{-1}$ K$^{-1}$) | $C_P$ (J kg$^{-1}$ K$^{-1}$) | $\rho_i$ (kg m$^{-3}$) |
|---|---|---|---|
| Negative electrode | 1.04 | 1437.4 | 1347.3 |
| Positive electrode | 1.58 | 1269.2 | 2328.5 |
| Separator | 0.344 | 1978.16 | 1009 |
| Electrolyte | 0.6 | 2055 | 1130 |
| Copper, Cu | 398 | 385 | 8933 |
| Aluminium, Al | 170 | 875 | 2770 |
| Battery can | 44.5 | 475 | 7850 |
| Battery mandrel (Nylon) | 0.26 | 1700 | 1150 |
| Battery active material (total) | 45.01(angular)<br>1.1855(radial) | 1284.4 | 2422.2 |

The battery consists of electrodes and a separator twisted into a cylinder in multiple layers. This is why the battery model's heat conductivity is anisotropic. For the current geometry of the 18650 LFP cell, the thermal conductivity is higher in the axial direction than in the radial direction[67].Thermal properties of materials are showing at Table 3. Therefore, the following describes the heat conductivity in both the radial and axial directions:

$$k_{T,r} = \frac{\sum L_i}{\sum (L_i/k_{T,i})},\ k_{T,\text{ang}} = \frac{\sum L_i k_{T,i}}{\sum L_i} \tag{34}$$

Nevertheless, the battery cylinder is cantered at the origin and extrudes in the z-direction because of the cartesian coordinate system. The thermal conductivity of the active material in the cell in the x, y, and z directions is defined as follows[67].

$$k_{T,x} = \frac{|y|}{r}\frac{\sum L_i k_{T,i}}{\sum L_i} + \frac{|x|}{r}\frac{\sum L_i}{\sum L_i/k_{T,i}} \tag{35}$$

$$k_{T,y} = \frac{|x|}{r}\frac{\sum L_i k_{T,i}}{\sum L_i} + \frac{|y|}{r}\frac{\sum L_i}{\frac{\sum L_i}{k_{T,i}}},\ k_{T,z} = \frac{\sum L_i k_{T,i}}{\sum L_i} \tag{36}$$

The equation below represents the total density of the active material in the cell:

$$\rho = \frac{\sum L_i \rho_i}{\sum L_i} \tag{37}$$

The equation below represents the heat capacity of the active material in the cell[67]:

$$C_p = \frac{\sum L_i C_{p,i}}{\sum L_i} \tag{38}$$

### 4.3.3 Electrochemical-Thermal Model coupling

In this study, a coupled framework is employed to integrate the electrochemical and thermal models for accurately simulating the behaviour of a cylindrical battery. The electrochemical model, which operate in one dimension, calculates key variables such as the solid and liquid potentials ($\phi_s$, $\phi_l$), ionic concentrations ($C_s$,$C_l$), and the heat generation rate ($Q_h$) The heat generation arises from both irreversible processes (e.g., overpotentials) and reversible processes (e.g., entropy changes). This heat generation rate is passed to a three-dimensional thermal model, which predicts the spatial temperature distribution (T) within the battery. The updated temperature field is then fed back into the electrochemical model to adjust temperature-dependent parameters such as reaction rates and transport properties, ensuring a self-consistent solution. Fig. 4.5 illustrates this iterative coupling process, where heat generation and temperature distributions are exchanged between the models. ($Q_{h,2D}$)

The heat generation computed by the electrochemical model in two dimensions is scaled to three dimensions using the following equation:

$$Q_{h,3D} = Q_{h,2D} \times \frac{L_{neg} + L_{sep} + L_{pos}}{L_{batt}} \times \frac{\left((r_{batt} - d_{can})^2 - r_{mandrel}^2\right)(h_{batt} - 2d_{can})}{(r^2\ batt - r_{mandrel}^2)h_{batt}} \tag{39}$$

This coupling framework enables the models to capture the mutual dependence of heat generation and temperature on electrochemical and thermal behaviours. By iteratively exchanging ($Q_h$) and T, the framework ensures that spatial temperature gradients and their effects on battery performance, efficiency, and safety are accurately resolved. This approach is essential for understanding the thermal dynamics of batteries, particularly under high-stress or abusive operating conditions.

We have explained the electrochemical and heat transfer models and how they are connected, as shown in Fig. 4.5. During the operation of a lithium-ion battery (LIBs), heat generation increases the temperature inside the battery. This change in temperature affects the electrochemical reactions, which then influence the amount of heat produced. This interaction creates a feedback loop, making it necessary to couple the thermal and electrochemical models.

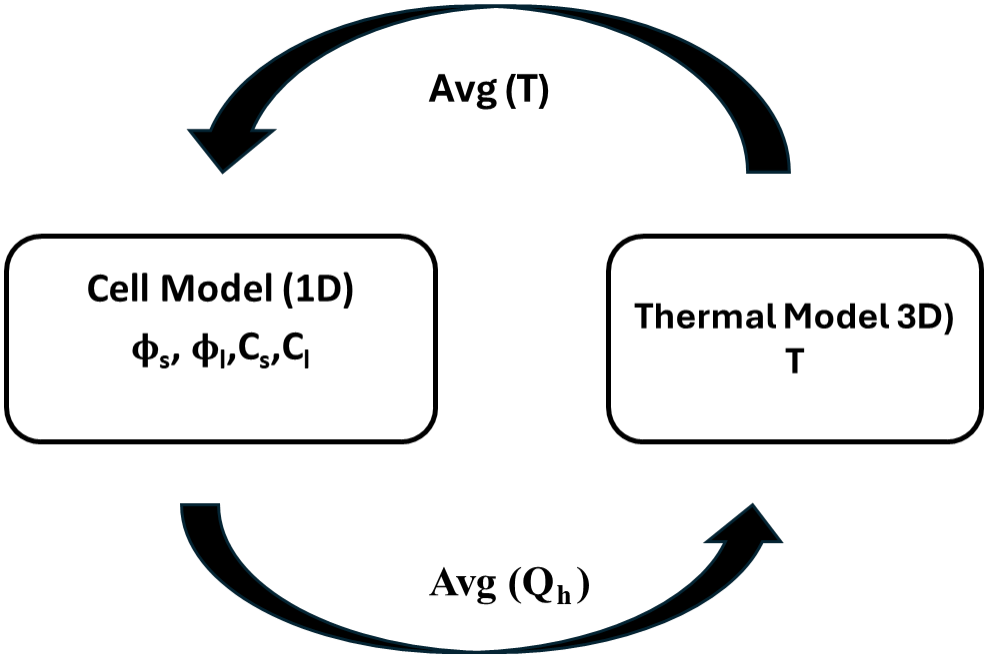


Figure 4.5 Electrochemical-Thermal coupling model

To make the model more realistic and accurate, we include parameters that depend on temperature and lithium concentration. The two main parameters are:

Diffusion Coefficient $(D_s)$ , represents how lithium ions move within the active material, changing with temperature. The relationship is given by the Arrhenius equation[63]:

$$D_{s,n} = D_{s,n}^{0}\exp\left\{\frac{E_{d,n}}{R}\left(\frac{1}{T^0}-\frac{1}{T}\right)\right\} \tag{40}$$

$$D_{s,p} = \frac{D_{sp}^{\rho}}{\left(1+SOC_p\right)^{1.6}}\left\{\frac{E_{d,p}}{R}\left(\frac{1}{T^0}-\frac{1}{T}\right)\right\} \tag{41}$$

Reaction Rate Constant $(k)$ describes the speed of the electrochemical reactions and depends on temperature, following a similar equation:

$$k_n = k_n^{0}\exp\left\{\frac{E_{k,n}}{R}\left(\frac{1}{T^0}-\frac{1}{T}\right)\right\} \tag{42}$$

$$k_p = k_p^{0}\exp\left(-3soc_p\right)\exp\left\{\frac{E_{k,p}}{R}\left(\frac{1}{T^0}-\frac{1}{T}\right)\right\} \tag{43}$$

# Chapter 5

## Result & Discussion

## 5.1 Model Validation

### 5.1.1 Evolutions of the cell potential

*Figure 5.1* exhibits the results of comparing experimental and simulated results across different discharge rates (C-rates: 0.5C, 1C, 2C, and 3C) to validate the performance of the battery model. For voltage versus capacity *Figure 5.1* (a), there is a strong agreement between the experimental data (circular markers) and the simulation results (solid lines). This shows that the model can accurately capture the behaviour of the battery under different operating conditions. At lower C-rates (0.5C and 1C), the simulation faithfully reproduces the steady-state voltage observed in the experimental data over time and capacity. This shows that the electrochemical and transport processes at lower discharge rates are well-represented by the model. Nonetheless, minor differences are seen in both graphs at higher C-rates (2C and 3C). The simulated voltage is higher than the experimental data in the mid-discharge region, as shown by the higher predicted voltage for a given capacity (*Figure 5.1*(a)). These deviations are likely due to increased polarization, ohmic resistance, and diffusion limitations, which become stronger at higher current rates. Both simulated and experimental results consistently show a sharp voltage drop toward the end of discharge, which suggests that the active material is being depleted. The main cause of the voltage drops during discharge, particularly near the end of the discharge process, is the rise in internal resistance. Matrix resistance, kinetic resistance, diffusion resistance, solution resistance, and contact resistance between the electrode and the current collector comprise the internal resistance of the cell. The voltage-capacity relationships show that these resistances contribute to energy losses and steep voltage declines, which become more apparent at higher C-rates. Additionally, both figures show that the overall capacity decreases as the C-rate increases. The model correctly predicts the decrease in active material utilization at higher discharge currents, reflected in this reduction.

In *Figure 5.1*(b), error analysis is presented in the bar graphs to determine the model accuracy at various C-rates. The average percentage error rises from less than 1% at 0.5C to about 1.2% at 3C, and the root mean square (RMS) error from about 36 mV at 0.5C to 62 mV at 3C. However, the low RMS error at all C-rates support the general conclusion that the model is accurate.

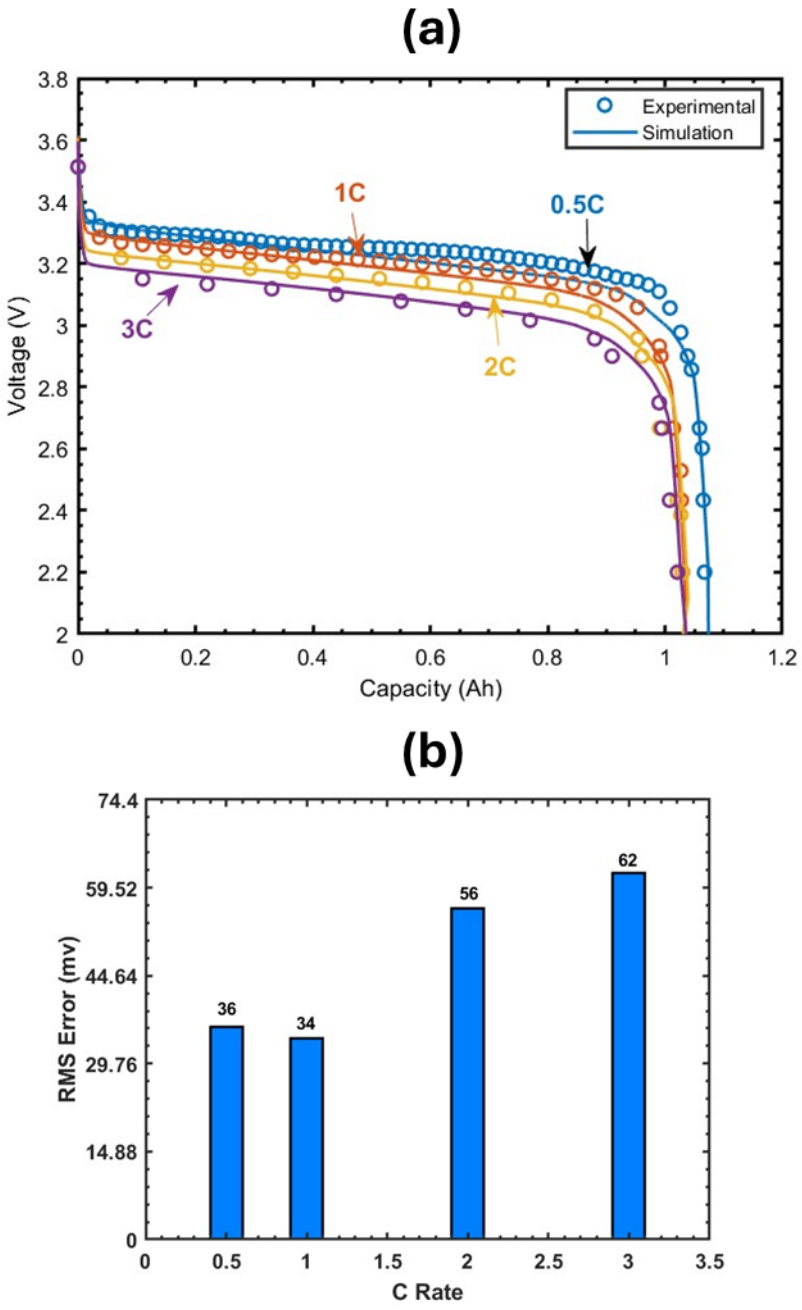


Figure 5.1 Comparison between an experiment and simulation at a different discharge rate of (a) Voltage (v) vs Capacity (Ah) (b) error(mv) between an experiment and simulation at a different discharge rate

### 5.1.2 Evolutions of the cell temperature

To find the fidelity of the P2D electrochemical-thermal coupling model, we compared simulation data of the surface temperature of 18650 cylindrical cells consisting of LiFeO4 cathode and graphite anode with open-source experimental data by Sandia National Laboratory (SNL) [58]. *Figure 5.2* illustrates the experimental and simulated average surface temperature of 18650 cells at different C-rates (1C, 2C, and 3C). Fig 5.2 compares the temperature difference, ΔT (K) as a function of time(s), while Fig 5.3 provides temperature contour plots for the cell cross-section under these conditions.

In *Figure 5.2*(a), The temperature difference, ΔT-time (s) plots show that at 1C, the temperature difference remains minimal throughout the discharge process, with excellent agreement between experimental and simulated results. The temperature rises as the C-rate increases to 2C and 3C, reflecting the higher heat generation associated with greater current densities. Although slight deviations are observed at 3C, the model effectively captures these trends, where it underestimates the experimental temperature difference, ΔT(K), in the mid-discharge region. It shows that the average Temperature difference between the cell and the environment increased at the end of discharge. The reason for this large polarization is at the end of discharge. Also, the temperature difference increased as the C rate increased. The temperature difference increased in 1C from 0K to 1.6342K, and in 2C from 0K to 2.3312K at 3C, it increased from 0K to 5.14K at the end of the discharge process. This is because more heat is generated at a high C rate as it works with a high current flow, raising internal resistance and producing more heat in the battery. However, few deflections are shown between experimental and simulation results. In *Figure 5.2*(b) The error analysis is presented in the bar graphs to determine the model accuracy at various C-rates. The root mean square (RMS) error of the simulation results with respect to the experiment ranges from about 0.24K at 1C to 0.21K at 3C.

*Figure 5.3* provides further insight into the thermal behaviour through temperature contour plots for the end of discharge at 1C, 2C, and 3C. At 1C, the temperature distribution across the cell is relatively uniform, with a maximum temperature of approximately 1.67 K near the centre of the cell. However, at higher C-rates, the maximum temperature increases to 2.38 K at 2C and 5.14 K at 3C, with the heat concentrated along the cell's core. This non-uniform distribution reflects the dominance of resistive heating (Joule heating) and polarization losses, which intensify at higher current densities. The contours also reveal that the outer layers of the cell remain relatively cooler. At the same time, the core experiences the highest temperature rise due to poor thermal conductivity in the radial direction.

These observations confirm that the temperature rise is primarily driven by internal resistances, including Joule heating and polarization losses, which become more significant as the C-rate increases. The model successfully predicts the overall temperature trends and spatial distributions, validating its reliability for simulating thermal behaviour. However, minor deviations at higher C-rates highlight the need for further refinement to account for localized heat transfer effects and material properties. Overall, the combination of Temperature difference(K)-time(s) and temperature contour analysis demonstrates the model's capability to predict the thermal characteristics of 18650 cells under varying operating conditions.

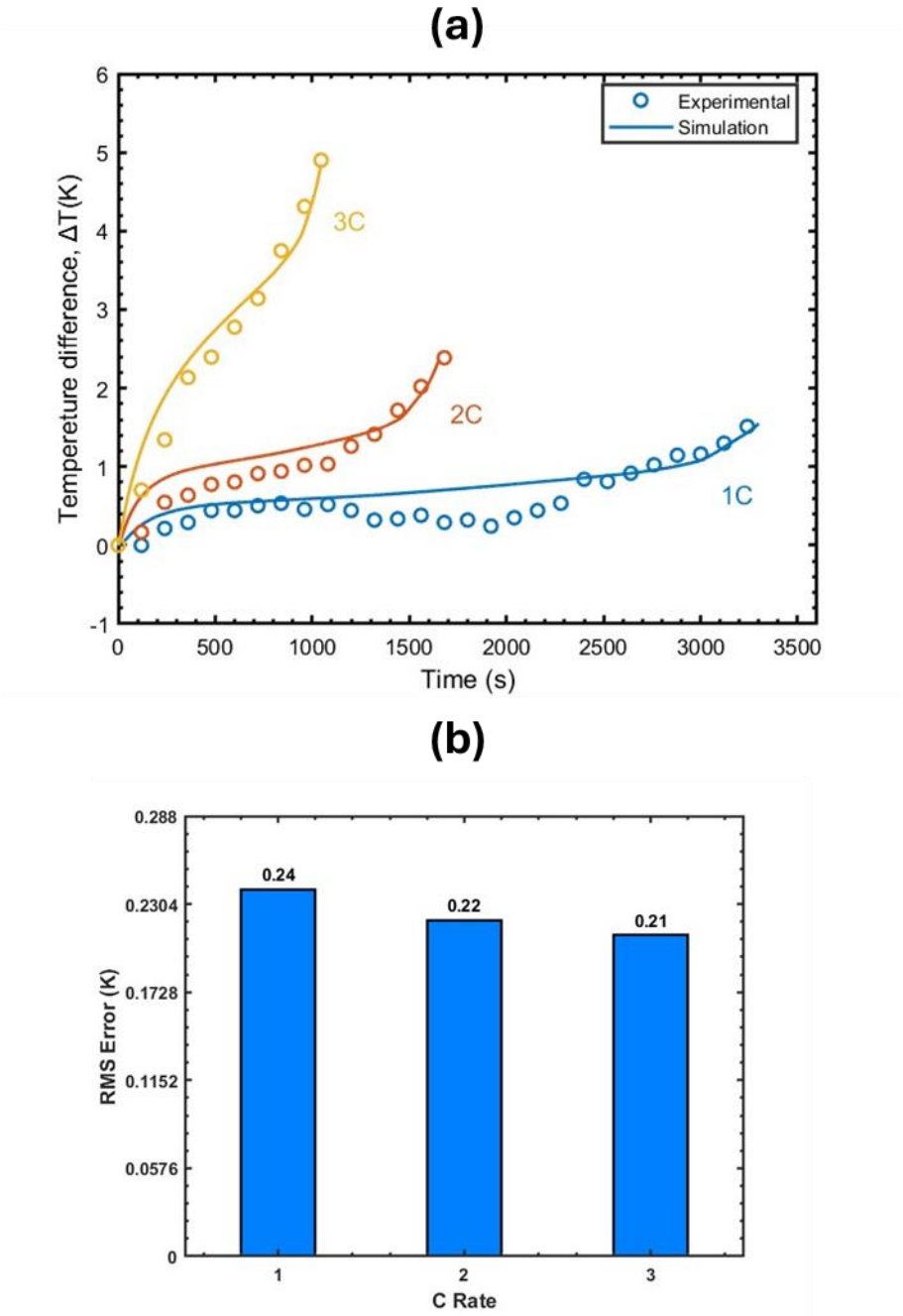


Figure 5.2: Comparison between an experiment and simulation at a different discharge rate of (a) Temperature (v) vs time (s), (b) error(K) between an experiment and simulation at a different discharge rate

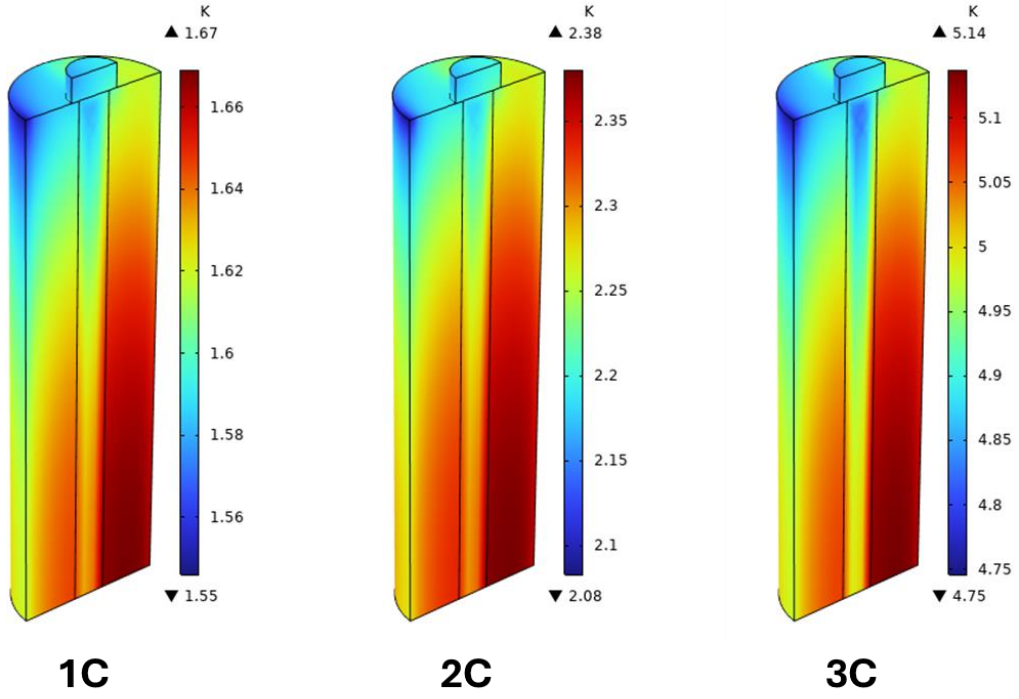


Figure 5.3 Temperature contour of the standard 18650 LFP cell at the end of 1C,2C,3C discharge

## 5.2 Effect of adding electrolyte channel

Adding an Electrolyte channel to the electrode surface increases the contact surface area between the electrode and electrolyte, increasing the Li ion's rate transfer capability. Adding electrolyte channels increases contact between the electrode and the electrolyte; internal resistance decreases, and ion transport becomes easy. This better ion movement will reduce the heat generated through the charging and discharging processes, which will likely enhance the battery's thermal behaviour by generating less heat. This better ionic flow battery reduces energy loss. So, it can be kept at a stable temperature, and the chance of overheating is lower. However, internal resistance is higher during fast discharging due to the rapid movement of ions. So, temperature fluctuations can be shown. That is why optimum electrolyte design parameters are needed. However, adding an electrolyte channel removes more active materials from the battery, which can lead to decreased battery performance. So, it is necessary to do an optimum design that will not reduce battery performance and temperature difference and make it more thermally efficient. Various channel widths, thicknesses, and channel number ranges were analysed to find this optimum value.

### 5.2.1 Effect of Channel Width

This study evaluated the effect of varying channel widths in the electrodes (both electrodes, positive electrode, and negative electrode) on the temperature and capacity of lithium-ion batteries. The addition of electrolyte channels reduces the volume of active material, thereby influencing electrochemical performance. To minimize this impact, channel widths were designed at the nanometer scale, appearing as dot-like structures within the electrodes.

Initially, the channel thickness was constant at 50 µm, while the width was varied from 0 nm to 100 nm to investigate its influence. The results are presented through temperature contour plots *Figure 5.5*(a-c) and graphs *Figure 5.4* (a-f), highlighting the role of channel width in controlling cell temperature differences and capacity at the end of discharge.

The graphs *Figure 5.4*(a, c, e) illustrate the average temperature difference (ΔT) across all active materials, determined using a domain probe and integration method. The temperature difference was calculated as $\Delta T = T - T_{inlet}$, with $T_{inlet}$=298.15 K. Contour plots *Figure 5.5*(a-c) provide further insights into the thermal behavior, showing variations in maximum and minimum temperature differences and temperature flow within the cell at the end of a 3C discharge.

The results indicate that wider channels (100 nm) dissipate heat more uniformly but reduce the volume of active material, while narrower channels (e.g., 10 nm) lead to uneven heat with hotspots. At a 1C discharge rate, adding channels did not improve thermal performance significantly, and no discernible pattern in temperature changes was observed across the three designs. The inclusion of 75 nm channels in both electrodes resulted in a maximum temperature difference of 1.88 K shown in *Figure 5.4*(a).

At higher discharge rates, such as 2C and 3C, electrolyte channels demonstrated improved thermal performance. For a 2C discharge showing in *Figure 5.4*(c) Using channels in the negative electrode with widths ranging from 0 nm to 50 nm decreased the temperature difference, reaching a minimum of 2.20 K at 50 nm. Beyond 50 nm, temperature differences began to increase again. A similar trend was observed when channels were introduced in both electrodes, with the lowest temperature difference being 2.23 K at 50 nm. However, channels in the positive electrode alone showed no significant effect on temperature.

At a 3C discharge rate, *Figure 5.4*(e), the best thermal performance was achieved with a 50 nm channel in the negative electrode, yielding a temperature difference of 4.876 K. Channels in both electrodes and the positive electrode also reduced the temperature difference, but no consistent trend was evident.

The capacity results showing in *Figure 5.4*(b, d, f) followed a similar pattern to the thermal results. At 1C, capacity variations did not show a clear trend across all designs. At 2C, the standard cell exhibited slightly higher capacity, while the addition of channels caused a capacity drop across all widths, without a significant pattern. For a 50 nm channel width in the negative electrode, the capacity was recorded at 1.0065 Ah. At 3C, the capacity decreased for all designs, attributed to the rapid movement of Li-ions, which limited the time available for deintercalation, diffusion, and intercalation. For a 50 nm channel width in the negative electrode, the capacity was found to be 0.95975 Ah.

Negative electrode channels were especially effective in regulating temperature and maintaining capacity, as they facilitated better heat conduction and reduced thermal differentials while preserving the use of active material. In contrast, channels in the positive electrode alone led to significant temperature increases and were less effective. These results highlight the advantages of negative or dual-electrode channel designs for optimizing both thermal and electrochemical performance.

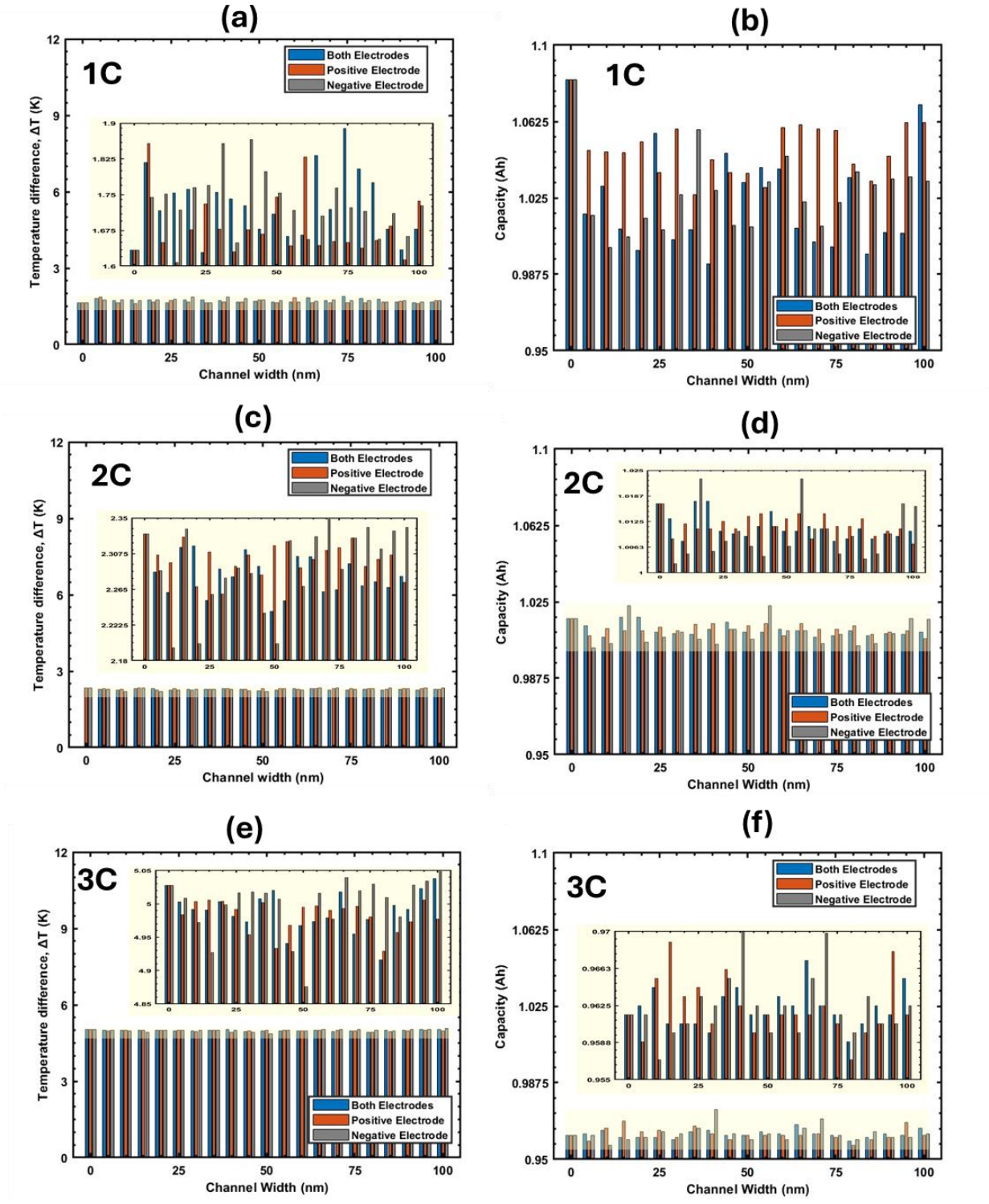


Figure 5.4 The performance of adding electrolyte channel width for (a), (c), (e) temperature difference (K) and (b), (d), (f) capacity (Ah)

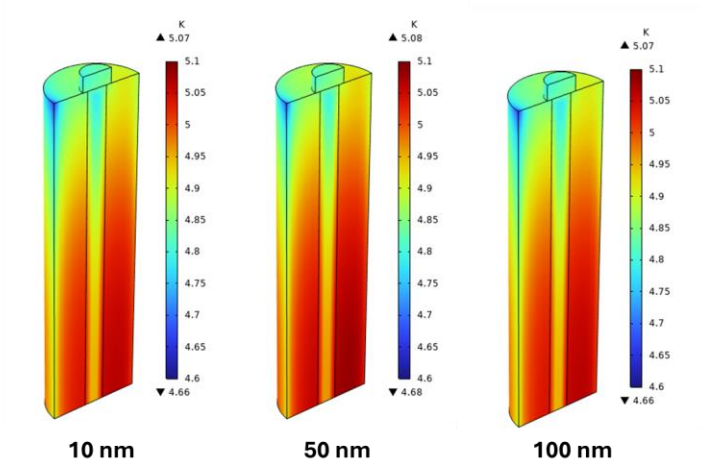


(a) Both Electrodes

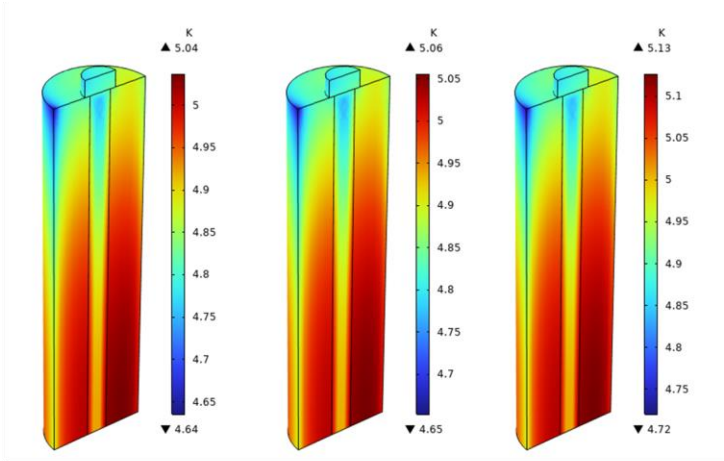


(b) positive Electrode

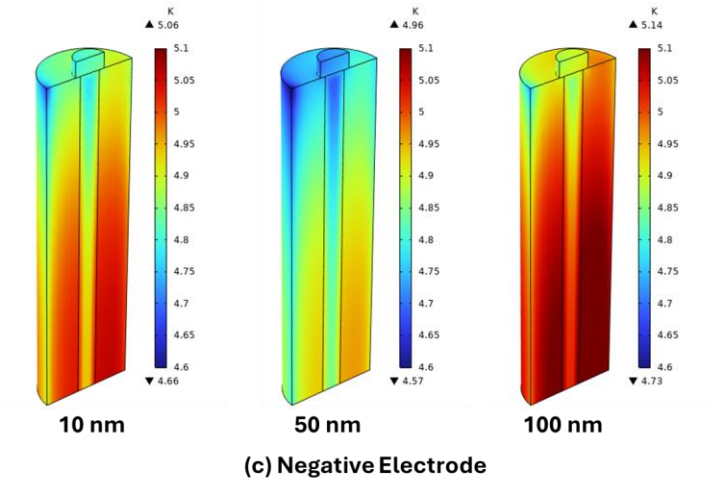


(c) Negative Electrode

Figure 5.5 Temperature contour of the 18650 LFP cell at the end of 3C discharge with various electrolyte channel widths from 10nm to 100nm: (a) both electrodes, (b) positive electrode, (c) negative electrode.

## 5.3 Effect of Channel Thickness

This study explored the effects of channel thicknesses ranging from 0 to 10 µm, with a fixed channel width of 50 nm, on lithium-ion batteries' thermal and electrochemical performance under discharge rates of 1C, 2C, and 3C. The thermal response was analysed using the average temperature difference ($T - T_{inlet}$). $T_{inlet}$ was set at 298.15 K. The findings are presented in temperature contour plots (*Figure 5.7*(a-c) and graphs (*Figure 5.6*(a-f), which illustrates the impact of channel thickness on temperature and capacity across three configurations: channels in the negative electrode, positive electrode, or both electrodes.

At the 1C discharge rate showing in *Figure 5.6*(a), introducing channels across the three configurations yielded no significant thermal advantages. The average temperature rise varied inconsistently, with no clear patterns observed across designs.

At the 2C discharge rate shown in *Figure 5.6* (c), the effect of channel thickness became more noticeable. For the negative electrode, the average temperature difference decreased as the channel thickness increased from 0 µm to 5 µm, reaching a minimum of 2.20 K, which marked a 5.6% reduction compared to the standard cell. Beyond 5 µm, the temperature difference began to rise again, though without a consistent trend. For channels in both electrodes, the minimum temperature difference was 2.238 K at 5 µm, corresponding to a 3.9% reduction. Channels in the positive electrode also reduced temperature differences but to a lesser extent and without a clear trend.

At the 3C discharge rate showing in *Figure 5.6*(e), channels in the negative electrode and both electrodes effectively reduced temperature differences, while those in the positive electrode increased it. The best thermal performance was achieved with a 5 µm channel thickness in the negative electrode, yielding a temperature difference of 4.876 K, a 3% reduction. Similarly, channels in both electrodes showed optimal performance at 5 µm, with a temperature difference of 4.967 K, equating to a 1.3% reduction. Temperature contour plots (*Figure 5.7*) showed uneven heat distribution across the electrodes, but the role of channel thickness became more evident at higher discharge rates (2C and 3C).

The capacity results showing *Figure 5.6*(b, d, f) reflected similar trends to the thermal performance. At 1C, capacity variations lacked a clear pattern across all configurations. At 2C, the standard cell showed slightly higher capacity, while adding channels caused capacity reductions across all thicknesses without a discernible trend. A 5 µm channel thickness in the negative electrode resulted in a capacity of 1.0065 Ah. At 3C, capacity decreased across all designs due to the rapid movement of Li-ions, limiting the time for deintercalation, diffusion, and intercalation. For a 5 µm channel thickness in the negative electrode, the capacity was measured at 0.95975 Ah.

A 5 µm channel thickness in the negative electrode proved optimal, minimizing temperature differences and maintaining stable capacity, particularly at high C-rates like 3C. While both-electrode channels were effective, channels in the positive electrode increased temperatures and reduced capacity, highlighting the need for careful channel design.

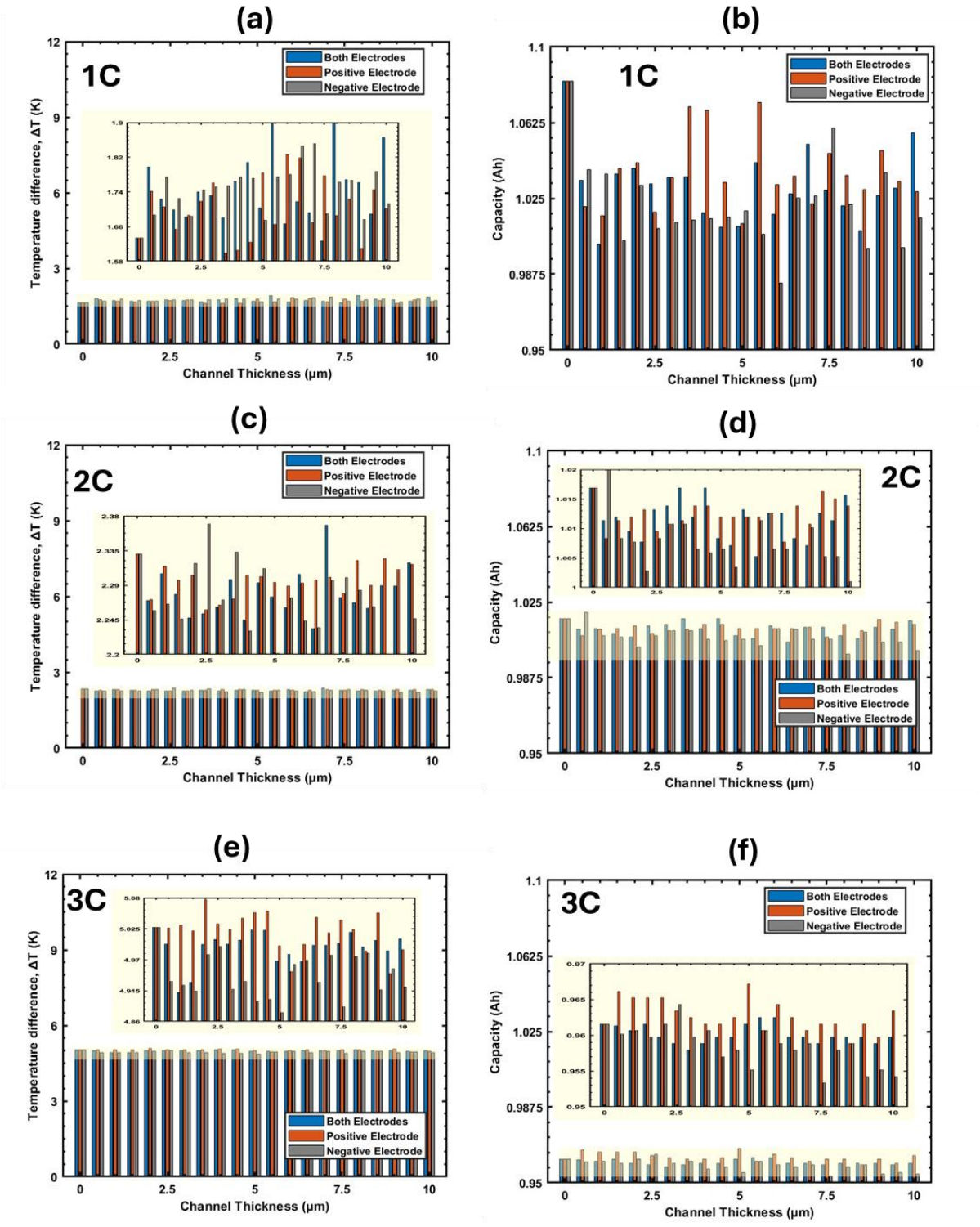


Figure 5.6 The performance of adding electrolyte channel thickness for (a), (c), (e) temperature difference (K) and (b), (d), (f) capacity (Ah) difference

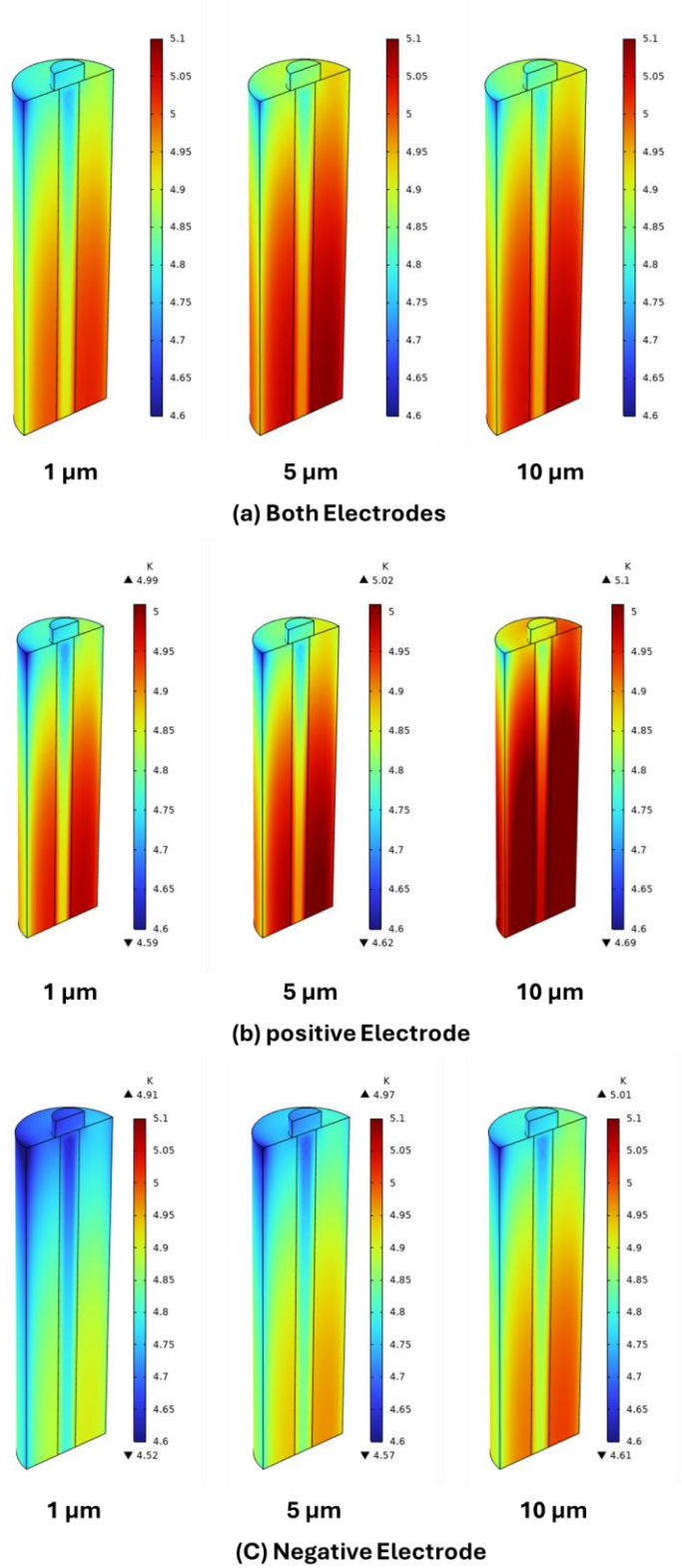


Figure 5.7 Temperature contour of the 18650 LFP cell at the conclusion of a 3C discharge with various electrolyte channel thicknesses from 1 µm to 10 µm: (a) both electrodes, (b) positive electrode, (c) negative electrode.

## 5.4 Effect of Channel number

This study investigates the influence of varying the number of electrolyte channels, ranging from one to eight, on a lithium-ion battery's thermal and electrochemical performance under discharge rates of 1C, 2C, and 3C. The analysis focuses on temperature difference(K) and capacity, identifying the optimal configuration of five channels in the negative electrode. The results are visualized in temperature contour plots *Figure 5. 9* (a-c) and performance graphs *Figure 5.8* (a-f), which examine the effects of channel number under three configurations: channels in the negative electrode, positive electrode, or both electrodes.

At the 1C discharge rate, the addition of channels across all configurations had a minimal impact on performance. Temperature differences showed no significant reduction or discernible trend, as illustrated in *Figure 5.8*(a). Similarly, capacity variations at 1C lacked a consistent pattern across all designs, as shown in *Figure 5.8*(b). This indicates that at lower discharge rates, the introduction of channels does not provide notable thermal or electrochemical benefits.

At 2C, the effects of channel number became more evident. For the negative electrode, increasing the number of channels from 0 to 5 reduced the average temperature difference (K) 2.135 K, representing an 8.4% decrease compared to the standard cell. However, adding more than five channels did not further improve performance and sometimes increased the temperature difference. Capacity also followed a similar trend; the standard cell exhibited slightly higher capacity compared to configurations with added channels, but with five channels in the negative electrode, the capacity stabilized at 1.001 Ah at *Figure 5.8*(d).

At the 3C discharge rate, where heat generation is at its peak, the advantages of five channels in the negative electrode became more pronounced. With fewer channels, the temperature difference reached approximately 4.87 K, while the five channels reduced this to 4.75 K, as shown in *Figure 5.8*(e). Beyond the five channels, performance declined, likely due to disruptions in heat dissipation and ion transport caused by excessive channeling. Capacity also peaked with five channels, achieving 0.957 Ah at *Figure 5.8*(f). Adding more channels led to a slight capacity drop, attributed to the excessive division of the active electrode area.

Channels in both electrodes also contributed to temperature reduction. The temperature difference decreased to 4.9378 K with five channels in both electrodes. However, this configuration did not offer significant advantages over the negative electrode-only design. Conversely, for channels in the positive electrode, the temperature difference remained higher regardless of the number of channels, making this configuration less effective.

The thermal analysis highlights five channels in the negative electrode as the optimal design. This effectively minimizes temperature differences, evenly distributes heat, and maintains stable capacity, particularly at high C-rates like 2C and 3C. Adding more than five channels disrupts thermal and ion flow, reducing efficiency, while fewer channels lead to hotspots and uneven heat dissipation. This emphasizes the importance of balanced channel design for optimal battery performance.

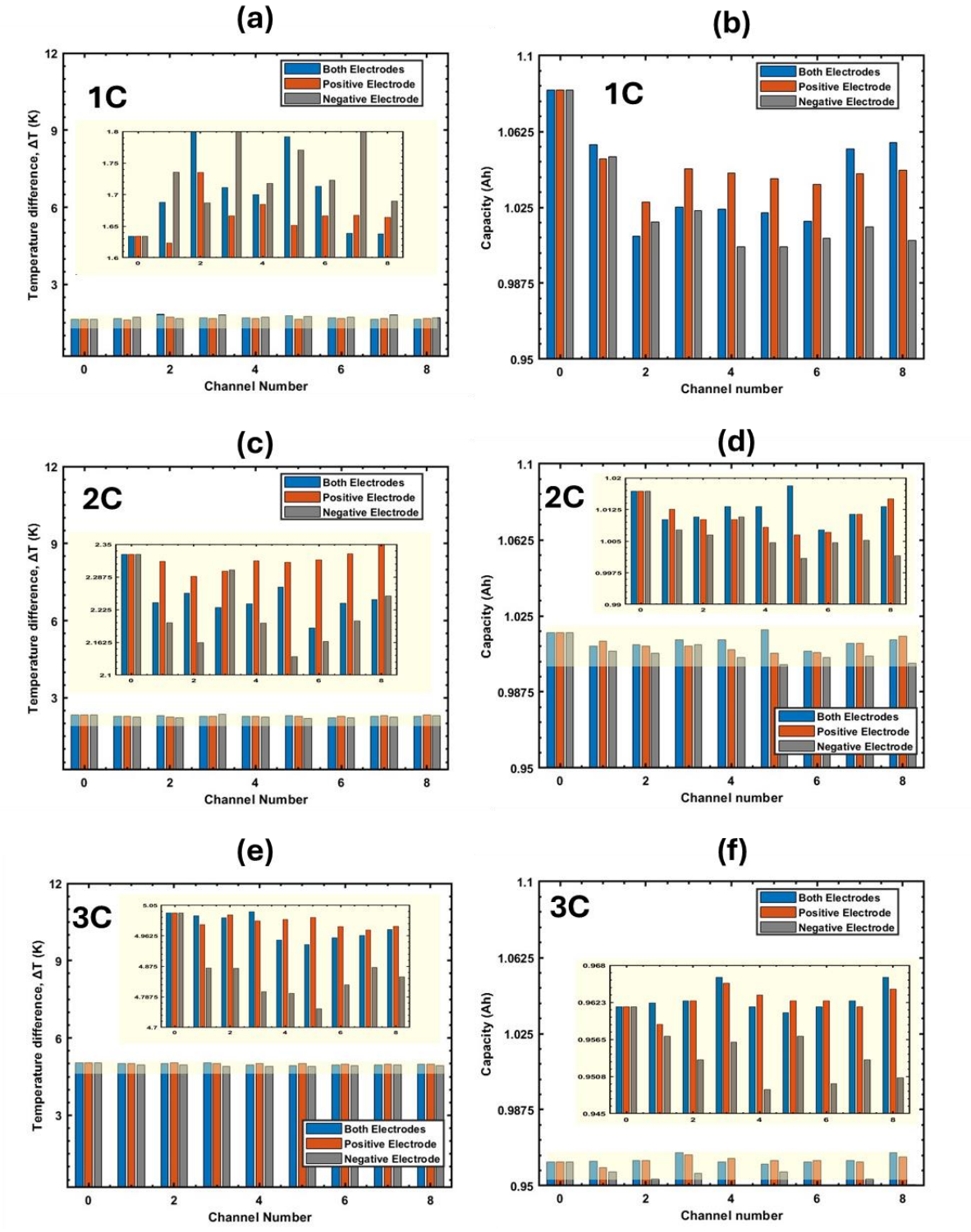


Figure 5.8 The performance of adding electrolyte channel number for (a), (c), (e) temperature difference (K) and (b), (d), (f) capacity (Ah) variations

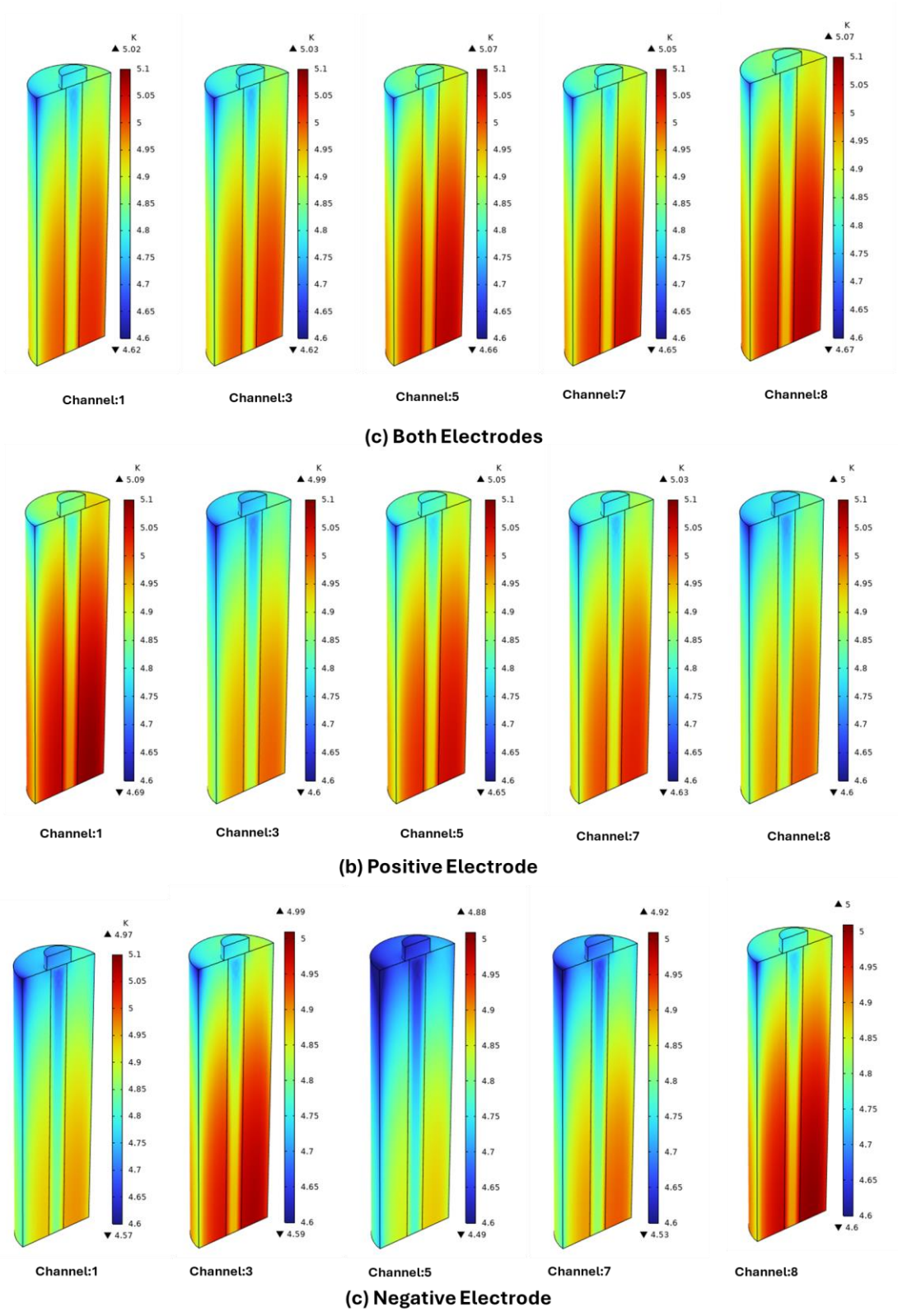


Figure 5. 9 Temperature contour of the 18650 LFP cell at the end of a 3C discharge with various electrolyte channel numbers from 1 to 8: (a) both electrodes, (b) positive electrode, (c) negative electrode.

# Chapter 6

## Conclusion

This study presents a P2D electrochemical model coupled with a thermal model to design bio-inspired electrodes by adding electrolyte channels in 2D design for commercial A123 system 18650 LFP batteries. Numerical analysis was done by using COMSOL Multiphysics battery design module version 6.2. Data analysis and plot generation were analysed using the MATLAB 2024b version. The accuracy and reliability of this model analysis are measured by comparing numerical data with experimental data. Also, the electrolyte channel effect on thermal performances was analysed. The main conclusions of this work are summaries as follows:

1. Adjusting the width of the electrolyte channel from 0 to 100 nm in 3 different types of cell design (both electrodes, anode, and cathode) significantly influences thermal and electrochemical performance. We observe optimal performance at a 50 nm channel width in the negative electrode, especially at higher C rates (2C and 3C), where we observe reductions in both the temperature difference and capacity. At 2C, the temperature difference decreases by 5.6%, from 2.33 K to 2.20 K, and at 3C, it decreases by 3.02%, from 5.028 K to 4.876 K. Capacity reductions at 50 nm are minimal, amounting to 0.9% at 2C and 0.2% at 3C, highlighting the effectiveness of this configuration in balancing thermal management and capacity retention. However, at lower C rates, the performance of the 50 nm configuration declines, with increased temperature differences and higher capacity reductions. On the other hand, a 75 nm channel width at 1C causes the temperature difference to rise by 15% and the maximum capacity to drop by 6%. This shows that thermal and electrochemical behaviour is not ideal at low C rates.
2. Keeping 50 nm width varying channel thickness from 0 to 10 µm in a 3-cell design. Adding a channel to the positive electrode has minimal effect while adding a channel to the negative electrode decreases both temperature and capacity. In the 1C of all cells, there was an increase in temperature, but no discernible pattern was observed in the decrease in capacity (Ah). However, in cells 2C and 3C, the temperature significantly decreased as the thickness increased, but the capacity decreased even more. Consequently, the 5 mm thickness channels in the negative electrode demonstrated optimal results at high C rates. In 2C, the temperature differences decreased from 2.33K to 2.20K, approximately 6%, while in 3C, the temperature differences decreased from 5.028K to 4.876K, approximately 3.1%. The capacity changes for cells 2C and 3C were 1% and 0.6%, respectively.
3. By maintaining a channel width of 50 nm and a channel thickness of 5 µm, incorporating 0 to 8 channels in various 3-cell configurations significantly improves performance under high C-rate conditions (2C and 3C). Increasing the number of channels in the negative electrode effectively reduces temperature rise, with a decrease of approximately 8.4% at 2C, from 2.33 K to 2.135 K, and about 5.45% at 3C, from 5.03 K to 4.75 K. These findings highlight the role of optimized channel design in enhancing thermal management during high-rate operations.

Overall, the findings from this study suggest that optimizing electrolyte channel design is crucial for enhancing the performance of lithium-ion batteries. The optimal design for reducing temperature differences, enhancing heat dissipation, and maintaining capacity stability, particularly at high C-rates, was five channels in the negative electrode with a 5 µm channel thickness and 50 nm width. This configuration strikes the best balance between efficient thermal management and effective electrochemical performance. These results provide a framework for designing advanced lithium-ion batteries with improved thermal and electrochemical stability, essential for the next generation of high-performance energy storage systems. The research highlights the importance of carefully selecting channel dimensions and configurations to achieve superior performance, especially in high-demand applications where thermal management is critical.

## Recommendations and future work

The thesis aims to determine the thermal performance of commercial 18650 Li-ion batteries. To address this research gap, a bio-inspired electrolyte channel design was proposed. We discovered that adding electrolyte channels can effectively lower the cell temperature during high-rate discharge. To find optimum design parameters, compare different ranges of width, thickness, and number of channel performances. Furthermore, this analysis presents a promising opportunity to improve the design of the electrolyte channel. Moreover, it provides the following research opportunity to enhance the battery's performance.

1. In this study, we exclusively examine the impact of temperature difference on the channel design of the electrolyte. Further research can discuss the effect of different types of heat generation processes, such as ohmic heat, polarization, reaction heat, etc., on this bio-inspired design.
2. To simplify numerical analysis, we used normalized cell height. We can analyze the actual size and check the thermal performance.
3. This bio-inspired design can be used to check the thermal performance of other types of batteries, such as pouch cells, button cells, and prismatic cells.
4. To check the overall performance of a commercial Li-ion cell using this bio-inspired design, electrochemical performance, energy density, power density, Li-ion plating, coulombic efficiency, etc., can be performed.

## List of References


[1] X. Hu *et al.*, "LRP-Based Design of Sustainable Recycling Network for Electric Vehicle Batteries," *Processes*, vol. 10, no. 2, Feb. 2022, doi: 10.3390/pr10020273.

[2] A. I. Osman *et al.*, "Cost, environmental impact, and resilience of renewable energy under a changing climate: a review," *Environ Chem Lett*, vol. 21, no. 2, pp. 741–764, Apr. 2023, doi: 10.1007/s10311-022-01532-8.

[3] F. Blaabjerg, "A comprehensive book about the future modern power grid with renewable sources-gives a lot of insight into the challenges and possibilities."

[4] "Electrolytes for Energy Storage Applications."

[5] B. Dunn, H. Kamath, and J.-M. Tarascon, "Electrical Energy Storage for the Grid: A Battery of Choices System power ratings, module size." [Online]. Available: https://www.science.org

[6] A. Jokar, B. Rajabloo, M. Désilets, and M. Lacroix, "Review of simplified Pseudo-two-Dimensional models of lithium-ion batteries," Sep. 30, 2016, *Elsevier B.V.* doi: 10.1016/j.jpowsour.2016.07.036.

[7] X. Zhang, "Thermal analysis of a cylindrical lithium-ion battery," *Electrochim Acta*, vol. 56, no. 3, pp. 1246–1255, Jan. 2011, doi: 10.1016/j.electacta.2010.10.054.

[8] Y. Chen *et al.*, "A review of lithium-ion battery safety concerns: The issues, strategies, and testing standards," Aug. 01, 2021, *Elsevier B.V.* doi: 10.1016/j.jechem.2020.10.017.

[9] M. Ahmadian-Elmi and P. Zhao, "Review of Thermal Management Strategies for Cylindrical Lithium-Ion Battery Packs," Feb. 01, 2024, *Multidisciplinary Digital Publishing Institute (MDPI)*. doi: 10.3390/batteries10020050.

[10] C. Forgez, D. Vinh Do, G. Friedrich, M. Morcrette, and C. Delacourt, "Thermal modeling of a cylindrical LiFePO4/graphite lithium-ion battery," *J Power Sources*, vol. 195, no. 9, pp. 2961–2968, May 2010, doi: 10.1016/j.jpowsour.2009.10.105.

[11] S. Baazouzi, N. Feistel, J. Wanner, I. Landwehr, A. Fill, and K. P. Birke, "Design, Properties, and Manufacturing of Cylindrical Li-Ion Battery Cells—A Generic Overview," *Batteries*, vol. 9, no. 6, Jun. 2023, doi: 10.3390/batteries9060309.

[12] S. Li, M. W. Marzook, C. Zhang, G. J. Offer, and M. Marinescu, "How to enable large format 4680 cylindrical lithium-ion batteries," *Appl Energy*, vol. 349, Nov. 2023, doi: 10.1016/j.apenergy.2023.121548.

[13] X. Hua *et al.*, "The prismatic surface cell cooling coefficient: A novel cell design optimisation tool & thermal parameterization method for a 3D discretised electro-thermal equivalent-circuit model," *eTransportation*, vol. 7, Feb. 2021, doi: 10.1016/j.etran.2020.100099.

[14] Z. Huang, H. Wang, T. Yang, W. Tian, T. Dong, and J. Wu, "Simulation of thermal behavior evolution in lithium-ion pouch cells using a coupled reaction-thermal-expansion model," *Appl Therm Eng*, vol. 217, Nov. 2022, doi: 10.1016/j.applthermaleng.2022.119255.

[15] W. A. Appiah, J. Park, S. Song, S. Byun, M. H. Ryou, and Y. M. Lee, "Design optimization of LiNi0.6Co0.2Mn0.2O2/graphite lithium-ion cells based on simulation and experimental data," *J Power Sources*, vol. 319, pp. 147–158, Jul. 2016, doi: 10.1016/j.jpowsour.2016.04.052.

[16] M. Singh, J. Kaiser, and H. Hahn, "Thick Electrodes for High Energy Lithium Ion Batteries," *J Electrochem Soc*, vol. 162, no. 7, pp. A1196–A1201, 2015, doi: 10.1149/2.0401507jes.

[17] M. Armand and J. M. Tarascon, "Building better batteries," Feb. 07, 2008. doi: 10.1038/451652a.

[18] S. Dhillon, G. Hernández, N. P. Wagner, A. M. Svensson, and D. Brandell, "Modelling capacity fade in silicon-graphite composite electrodes for lithium-ion batteries," *Electrochim Acta*, vol. 377, May 2021, doi: 10.1016/j.electacta.2021.138067.

[19] L. Schneider *et al.*, "Transport Properties in Electrodes for Lithium-Ion Batteries: Comparison of Compact versus Porous NCM Particles," *J Electrochem Soc*, vol. 169, no. 10, p. 100553, Oct. 2022, doi: 10.1149/1945-7111/ac9c37.

[20] H. Tao, G. Chen, C. Lian, H. Liu, and M. O. Coppens, "Multiscale modeling of ion transport in porous electrodes," *AIChE Journal*, vol. 68, no. 4, Apr. 2022, doi: 10.1002/aic.17571.

[21] J. W. Haverkort, "A theoretical analysis of the optimal electrode thickness and porosity," *Electrochim Acta*, vol. 295, pp. 846–860, Feb. 2019, doi: 10.1016/j.electacta.2018.10.065.

[22] P. Patel and G. J. Nelson, "The influence of structure on the electrochemical and thermal response of li-ion battery electrodes," *Journal of Energy Resources Technology, Transactions of the ASME*, vol. 142, no. 5, May 2020, doi: 10.1115/1.4045820.

[23] D. Wang, Y. Gao, X. Zhang, T. Dong, and C. Zhu, "A novel pseudo two-dimensional model for NCM Liion battery based on electrochemical-thermal coupling analysis," in *Proceedings - 2020 3rd International Conference on Electron Device and Mechanical Engineering, ICEDME 2020*, Institute of Electrical and Electronics Engineers Inc., May 2020, pp. 110–116. doi: 10.1109/ICEDME50972.2020.00031.

[24] S. Panchal, I. Dincer, M. Agelin-Chaab, R. Fraser, and M. Fowler, "Experimental and simulated temperature variations in a LiFePO4-20 Ah battery during discharge process," *Appl Energy*, vol. 180, pp. 504–515, Oct. 2016, doi: 10.1016/j.apenergy.2016.08.008.

[25] K. Shah *et al.*, "Modeling of steady-state convective cooling of cylindrical Li-ion cells," *J Power Sources*, vol. 258, pp. 374–381, Jul. 2014, doi: 10.1016/j.jpowsour.2014.01.115.

[26] K. Shah *et al.*, "An experimentally validated transient thermal model for cylindrical Li-ion cells," *J Power Sources*, vol. 271, pp. 262–268, Dec. 2014, doi: 10.1016/j.jpowsour.2014.07.118.

[27] P. Taheri, M. Yazdanpour, and M. Bahrami, "Transient three-dimensional thermal model for batteries with thin electrodes," *J Power Sources*, vol. 243, pp. 280–289, 2013, doi: 10.1016/j.jpowsour.2013.05.175.

[28] J. Kang, Y. Jia, G. Zhu, J. V. Wang, B. Huang, and Y. Fan, "How electrode thicknesses influence performance of cylindrical lithium-ion batteries," *J Energy Storage*, vol. 46, Feb. 2022, doi: 10.1016/j.est.2021.103827.

[29] S. Malifarge, B. Delobel, and C. Delacourt, "Experimental and Modeling Analysis of Graphite Electrodes with Various Thicknesses and Porosities for High-Energy-Density Li-Ion Batteries," *J Electrochem Soc*, vol. 165, no. 7, pp. A1275–A1287, 2018, doi: 10.1149/2.0301807jes.

[30] S. Baksa and W. Yourey, "Consumer-based evaluation of commercially available protected 18650 cells," *Batteries*, vol. 4, no. 3, Sep. 2018, doi: 10.3390/batteries4030045.

[31] V. Etacheri, R. Marom, R. Elazari, G. Salitra, and D. Aurbach, "Challenges in the development of advanced Li-ion batteries: A review," Sep. 2011. doi: 10.1039/c1ee01598b.

[32] M. J. Lain, J. Brandon, and E. Kendrick, "Design strategies for high power vs. High energy lithium ion cells," *Batteries*, vol. 5, no. 4, Dec. 2019, doi: 10.3390/batteries5040064.

[33] L. H. Saw, Y. Ye, and A. A. O. Tay, "Electrochemical-thermal analysis of 18650 Lithium Iron Phosphate cell," *Energy Convers Manag*, vol. 75, pp. 162–174, 2013, doi: 10.1016/j.enconman.2013.05.040.

[34] S. Panchal, M. Mathew, R. Fraser, and M. Fowler, "Electrochemical thermal modeling and experimental measurements of 18650 cylindrical lithium-ion battery during discharge cycle for an EV," *Appl Therm Eng*, vol. 135, pp. 123–132, May 2018, doi: 10.1016/j.applthermaleng.2018.02.046.

[35] T. Gao and W. Lu, "Physical Model and Machine Learning Enabled Electrolyte Channel Design for Fast Charging," *J Electrochem Soc*, vol. 167, no. 11, p. 110519, Jan. 2020, doi: 10.1149/1945-7111/aba096.

[36] P. Patel, G. Zhang, and G. J. Nelson, "Assessing the Impact of Electrode Structure on the Fast Charge Performance of Lithium-ion Batteries," *J Electrochem Soc*, vol. 170, no. 1, p. 010501, Jan. 2023, doi: 10.1149/1945-7111/acadb0.

[37] G. G. Wallace, J. Chen, A. J. Mozer, M. Forsyth, D. R. MacFarlane, and C. Wang, "Nanoelectrodes: energy conversion and storage," Jun. 2009. doi: 10.1016/S1369-7021(09)70177-4.

[38] K. Murashko, “Thermal modelling of commercial lithium-ion batteries,” 2016, doi: 10.13140/RG.2.1.3930.0723.

[39] L. Zou, F. Kang, X. Li, Y. P. Zheng, W. Shen, and J. Zhang, “Investigations on the modified natural graphite as anode materials in lithium ion battery,” *Journal of Physics and Chemistry of Solids*, vol. 69, no. 5–6, pp. 1265–1271, May 2008, doi: 10.1016/j.jpcs.2007.10.096.

[40] M. Yoshio, R. J. Brodd, and A. Kozawa, *Lithium-ion batteries: Science and technologies*. Springer New York, 2009. doi: 10.1007/978-0-387-34445-4.

[41] S. S. Zhang, “A review on the separators of liquid electrolyte Li-ion batteries,” Jan. 10, 2007. doi: 10.1016/j.jpowsour.2006.10.065.

[42] J. W. Fergus, “Recent developments in cathode materials for lithium ion batteries,” Feb. 15, 2010. doi: 10.1016/j.jpowsour.2009.08.089.

[43] X. He *et al.*, “Preparation of co-doped spherical spinel LiMn2O4 cathode materials for Li-ion batteries,” *J Power Sources*, vol. 150, no. 1–2, pp. 216–222, Oct. 2005, doi: 10.1016/j.jpowsour.2005.02.029.

[44] G. Saldaña, J. I. S. Martín, I. Zamora, F. J. Asensio, and O. Oñederra, “Analysis of the current electric battery models for electric vehicle simulation,” *Energies (Basel)*, vol. 12, no. 14, 2019, doi: 10.3390/en12142750.

[45] D. Aurbach *et al.*, “Design of electrolyte solutions for Li and Li-ion batteries: A review,” in *Electrochimica Acta*, Nov. 2004, pp. 247–254. doi: 10.1016/j.electacta.2004.01.090.

[46] S. T. Myung, Y. Sasaki, S. Sakurada, Y. K. Sun, and H. Yashiro, “Electrochemical behavior of current collectors for lithium batteries in non-aqueous alkyl carbonate solution and surface analysis by ToF-SIMS,” *Electrochim Acta*, vol. 55, no. 1, pp. 288–297, Dec. 2009, doi: 10.1016/j.electacta.2009.08.051.

[47] L. Hu *et al.*, “Interface engineering for enhancing electrocatalytic oxygen evolution of NiFe LDH/NiTe heterostructures,” *Appl Catal B*, vol. 273, Sep. 2020, doi: 10.1016/j.apcatb.2020.119014.

[48] Y. Preger *et al.*, “Degradation of Commercial Lithium-Ion Cells as a Function of Chemistry and Cycling Conditions,” *J Electrochem Soc*, vol. 167, no. 12, p. 120532, Jan. 2020, doi: 10.1149/1945-7111/abae37.

[49] D. H. Jeon and S. M. Baek, “Thermal modeling of cylindrical lithium ion battery during discharge cycle,” *Energy Convers Manag*, vol. 52, no. 8–9, pp. 2973–2981, Aug. 2011, doi: 10.1016/j.enconman.2011.04.013.

[50] M. Xiao and S. Y. Choe, “Theoretical and experimental analysis of heat generations of a pouch type LiMn2O4/carbon high power Li-polymer battery,” *J Power Sources*, vol. 241, pp. 46–55, 2013, doi: 10.1016/j.jpowsour.2013.04.062.

[51] M. Torchio, L. Magni, and R. B. Gopaluni, "A General Energy Balance for Battery Systems LIONSIMBA: A Matlab Framework Based on a Finite Volume Model Suitable for Li-Ion Battery Design, Simulation, and Control."

[52] Y. Ye, Y. Shi, N. Cai, J. Lee, and X. He, "Electro-thermal modeling and experimental validation for lithium ion battery," *J Power Sources*, vol. 199, pp. 227–238, Feb. 2012, doi: 10.1016/j.jpowsour.2011.10.027.

[53] M. Balasundaram, V. Ramar, C. Yap, L. Lu, A. A. O. Tay, and B. Palani, "Heat loss distribution: Impedance and thermal loss analyses in LiFePO4/graphite 18650 electrochemical cell," *J Power Sources*, vol. 328, pp. 413–421, Oct. 2016, doi: 10.1016/j.jpowsour.2016.08.045.

[54] Y. Lai *et al.*, "Insight into heat generation of lithium ion batteries based on the electrochemical-thermal model at high discharge rates," *Int J Hydrogen Energy*, vol. 40, no. 38, pp. 13039–13049, Oct. 2015, doi: 10.1016/j.ijhydene.2015.07.079.

[55] A. Nazari and S. Farhad, "Heat generation in lithium-ion batteries with different nominal capacities and chemistries," *Appl Therm Eng*, vol. 125, pp. 1501–1517, 2017, doi: 10.1016/j.applthermaleng.2017.07.126.

[56] S. Du *et al.*, "An investigation of irreversible heat generation in lithium ion batteries based on a thermo-electrochemical coupling method," *Appl Therm Eng*, vol. 121, pp. 501–510, 2017, doi: 10.1016/j.applthermaleng.2017.04.077.

[57] J. Esmaeili and H. Jannesari, "Developing heat source term including heat generation at rest condition for Lithium-ion battery pack by up scaling information from cell scale," *Energy Convers Manag*, vol. 139, pp. 194–205, 2017, doi: 10.1016/j.enconman.2017.02.052.

[58] "BatteryArchive.org." Accessed: Nov. 12, 2024. [Online]. Available: https://www.batteryarchive.org/

[59] Comsol, "Thermal Modeling of a Cylindrical Lithium-Ion Battery in 3D," 2021. [Online]. Available: www.comsol.com/trademarks.

[60] A. Fick, "Ueber Diffusion," *Ann Phys*, vol. 170, no. 1, pp. 59–86, 1855, doi: 10.1002/andp.18551700105.

[61] W. Dreyer, C. Guhlke, and R. Müller, "A new perspective on the electron transfer: Recovering the Butler-Volmer equation in non-equilibrium thermodynamics," *Physical Chemistry Chemical Physics*, vol. 18, no. 36, pp. 24966–24983, 2016, doi: 10.1039/c6cp04142f.

[62] Y. Wang and P. Wang, "Application of Fourier's Law in One-Dimensional Steady Heat Conduction Calculation of Cylinder Wall," in *Journal of Physics: Conference Series*, Institute of Physics, 2022. doi: 10.1088/1742-6596/2381/1/012002.

[63] J. Park, W. A. Appiah, S. Byun, D. Jin, M. H. Ryou, and Y. M. Lee, "Semi-empirical long-term cycle life model coupled with an electrolyte depletion function for large-

format graphite/LiFePO4 lithium-ion batteries," *J Power Sources*, vol. 365, pp. 257–265, 2017, doi: 10.1016/j.jpowsour.2017.08.094.

[64] M. Doyel, T. F.Fuller, and J. Newman, "Modeling of Galvanostatic Charge and Discharge of the Lithium/Polymer/Insertion Cell," *J. Electrochem. Soc.*, vol. Vol. 140, no. no.6, 1993.

[65] P. Nie *et al.*, "Full-cycle electrochemical-thermal coupling analysis for commercial lithium-ion batteries," *Appl Therm Eng*, vol. 184, Feb. 2021, doi: 10.1016/j.applthermaleng.2020.116258.

[66] G. Łukaszewicz and P. Kalita, "Stationary Solutions of the Navier–Stokes Equations," 2016, pp. 83–93. doi: 10.1007/978-3-319-27760-8_4.

[67] S.-C. Chen, Y.-Y. Wang, and C.-C. Wan, "Thermal Analysis of Spirally Wound Lithium Batteries," *J Electrochem Soc*, vol. 153, no. 4, p. A637, 2006, doi: 10.1149/1.2168051.